

A Raman Assay Method for the Enzymes Reacting with Gaseous
Substrates and its Application to Hydrogenase

「ガス状分子を基質とする酵素のためのラマン分光法を用
いた新規活性測定法の開発とヒドロゲナーゼへの応用」

2019

Yuka Kawahara-Nakagawa

中 川 由 佳

兵庫県立大学大学院生命理学研究科

Preface

Enzymes are macromolecules that efficiently catalyze various chemical reactions. The structures of enzymes are precisely optimized to achieve complex and difficult chemical reactions selectively with the least energy loss. It is quite difficult to create such a functional catalyst artificially. I am interested in the following questions: What happens in an enzyme during the catalytic reaction at the atomic level, and how does each building block of an enzyme relate to its function?

Unlike an artificial catalyst, an enzyme consists of protein moieties surrounding a catalytic active site. A substrate transport pathway, hydrogen-bonding networks with water molecules (proton pathways), an electron transport pathway, and an inhibitor/activator binding site are examples of such protein moieties. These protein moieties make it possible for enzymes to regulate multistep enzymatic reactions precisely. Their concerted mechanisms for controlling the rate and direction of the enzymatic reaction at the active site have not yet been fully elucidated.

In particular, hydrogenases are unique as they have three pathways: the gas channel (the substrate/product transport pathway), the proton pathway, and the electron transfer pathway. These pathways control the reversible conversion of molecular hydrogen (H_2) to protons (H^+) and electrons (e^-)—a simple but difficult reaction. The ultimate goal of this study is to determine how these pathways and the active site are conjugated during the enzymatic reaction. To answer this question, it is essential to perform kinetic analyses of two reactions catalyzed by hydrogenase *in vitro*: the H/D isotope exchange reaction and the *para/ortho* nuclear spin isomer conversion reaction. However, progress in this area of research has been very slow, presumably because conventional analytical methods (gas chromatography and mass spectrometry) are cumbersome and do not provide adequate data for detailed kinetic analysis. The crucial shortcoming of these conventional methods is that the substrate/products must be extracted from the reaction cuvette. This study has overcome this shortcoming by using Raman spectroscopy. I have developed a novel Raman spectroscopy-based assay system specifically to trace hydrogenase-mediated reactions continuously in a non-invasive manner. Using this system, the H/D exchange reaction catalyzed by the [NiFe] hydrogenase from *Desulfovibrio vulgaris* Miyazaki F (DvMF) was observed and the obtained data were subjected to kinetic analysis. The results provide information on the

relationship between the gas channel and the active site during the H/D exchange reaction.

Reliable and adequate Raman data were acquired by optimizing the spectrometer and all optical elements, and carefully removing possible sources of stray light which degrade the signal-to-noise ratio of Raman spectra. Moreover, a method was established for analyzing Raman spectra quantitatively, allowing precise understanding of the reaction mechanism. In addition, it was essential to optimize the preparation and handling of the enzyme to obtain reproducible results using hydrogenase. To this end, a reaction cuvette was developed that was tailored to these measurements.

Chapter 1 provides an overview of research on hydrogenases to date, and the usefulness and limitations of Raman spectroscopy applied to hydrogenase-mediated reactions are discussed. The development of both the Raman system and method for quantitative analysis of the spectral data are described in depth in Chapter 2. Detailed protocols and optimization of the experimental procedure, other than the development of Raman system, are discussed in Chapter 3. Chapter 4 focuses on measurements of the H/D exchange reaction catalyzed by [NiFe] hydrogenase using the newly developed Raman spectroscopy-based assay system. The results are analyzed using a reaction model and the mechanism of hydrogenase-mediated reactions is discussed. The final chapter of this thesis provides my conclusions and discusses the social significance and future perspectives of this study. Detailed experimental conditions and protocols pertaining to the Raman system are described in Chapter 2 and other aspects (mainly protocols for handling hydrogenase) are presented in Chapter 3. Important experimental conditions and protocols are summarized in the experimental section of Chapter 4.

The newly developed Raman method is potentially useful and applicable to other enzymes reacting with gaseous substrates. I hope that this research will contribute to the development of research on enzymes, and aid the future discovery of new chemical phenomena in enzymatic reactions and the development of high-performance catalysts.

Publication

Yuka Kawahara-Nakagawa, Koji Nishikawa, Satoru Nakashima, Shota Inoue, Takehiro Ohta, Takashi Ogura, Yasuteru Shigeta, Katsuyuki Fukutani, Tatsuhiko Yagi and Yoshiki Higuchi

New Assay Method Based on Raman Spectroscopy for Enzymes Reacting with Gaseous Substrates

Protein Science, **28** (2019) 663-670

Table of Contents

Preface	...1
Publication	...3
Table of Contents	...4
Chapter 1: General Introduction	...7
1-1 Hydrogenases	...8
1-1-1 Overview	...8
1-1-2 [NiFe] hydrogenase	...9
1-1-3 H/D exchange and nuclear spin conversion reactions of hydrogenases	...13
1-2 Raman spectroscopy	...15
1-2-1 Comparison between Raman spectroscopy and other analytical methods	...15
1-2-2 Raman spectroscopy for chemical analysis of reactions catalyzed by hydrogenase	...18
1-2-3 Shortcomings of Raman spectroscopy and strategies for overcoming them	...19
Chapter 2: Development of a Raman Spectroscopy-based Assay System	...20
2-1 Overview	...21
2-2 Development of the Raman system	...21
2-2-1 Spectrometer, detector, and laser	...21
2-2-2 Alignment of the optical elements	...24

2-2-3	Thermostatically controlled cuvette holder	...24
2-2-4	Fine alignment by optimizing the parameters and performance of the developed Raman system	...27
2-3	Establishment of a quantitative analysis method for Raman spectra	...31
2-4	Summary	...36
Chapter 3: Optimization of Experimental Protocols		...38
3-1	Overview	...39
3-2	Optimization of the experimental procedure	...42
3-2-1	Shape of the custom-built reaction cuvette	...42
3-2-2	Preparation of the enzyme solution	...43
3-2-3	Substitution methods for the gas phase	...45
3-2-4	Methods to initiate enzymatic reactions	...45
3-3	Optimized experimental methods for the H/D exchange assay	...48
3-4	Summary and future perspectives	...49
Chapter 4: Application of the Raman Spectroscopy-based Assay System to Hydrogenase		...51
4-1	Overview	...52
4-2	Materials and methods	...52
4-2-1	Materials and sample preparation	...52
4-2-2	Raman spectroscopy	...53
4-2-3	Assaying the H/D exchange reaction	...54
4-2-4	Data analysis	...54

4-3 Results	...57
4-3-1 Continuous monitoring of the catalytic reaction by Raman spectroscopy	...57
4-3-2 H/D exchange reaction in the D ₂ /H ₂ O system	...57
4-3-3 Effect of the product release rate from hydrogenase in the H/D exchange reaction using a kinetic model	...63
4-4 Discussion	...65
Chapter 5: Conclusion and Future Perspectives	...68
References	...72
Acknowledgements	...78
Appendices	...79
I: Comparison of the enzymatic activities of various hydrogenases	...79
II: Detailed explanation of the reaction model and equations used in Chapter 4	...81
List of Figures and Tables	...84

Chapter 1

General Introduction

1-1 Hydrogenases

1-1-1 Overview

Hydrogenases are a family of enzymes that efficiently catalyze the reversible conversion of molecular hydrogen (H_2) to protons (H^+) and electrons (e^-) under mild conditions.¹ The first hydrogenase was discovered by Stephenson *et al.* in 1931.² Using cells and/or cell extracts, three hydrogenase-mediated reactions have been investigated kinetically³⁻⁵: the reversible oxidation of molecular hydrogen, and two non-physiological reactions *in vitro*, namely, the H/D exchange reaction between $H^+(H_2O)/D^+(D_2O)$ and D_2/H_2 , and the nuclear spin isomer conversion reaction between *para*- H_2 and *ortho*- H_2 . These reactions have been reviewed in detail.⁶⁻⁸ Early studies concluded that hydrogenases cleave the bond in molecular hydrogen to generate a proton (H^+) and hydride (H^-) heterolytically.^{4,6} A detailed kinetic analysis by Yagi *et al.* in 1973 of H/D exchange and the nuclear spin isomer conversion reaction was the first to use highly purified hydrogenase from *Desulfovibrio vulgaris* Miyazaki F (DvMF).⁹ As other highly purified hydrogenases became available, kinetic studies were actively pursued to elucidate the enzymatic reaction mechanisms. For example, the substrate conversion processes catalyzed by hydrogenase were traced under various pH and temperature conditions, as well as various enzyme, substrate, and inhibitor/activator concentrations.¹⁰⁻¹² Hydrogenases from several species were mutated (i.e., specific amino acids were replaced with other amino acids) and their reaction rates were investigated to elucidate how specific amino acid residues are involved in the reaction.^{13,14} In addition to these kinetics studies, hydrogenases in several redox states have been investigated by spectroscopic methods such as Fourier transform infrared (FTIR), X-ray absorption spectroscopy, Mössbauer and electron paramagnetic resonance (EPR) to reveal the

structure and electronic state of the active site.^{1,15-17} It is currently known that there are three major types of hydrogenases ([NiFe], [FeFe], and [Fe] hydrogenases) based on the metal composition of the active site.¹ The first crystallographic structure of a [NiFe] hydrogenase, from *Desulfovibrio gigas*, was determined by Volbeda *et al.* in 1995,¹⁸ followed by its crystal structures in various redox states. Subsequent crystal structures revealed that [NiFe] and [FeFe] hydrogenases possess binuclear active sites, where one of the two atoms (Ni in [NiFe] hydrogenase and Fe in [FeFe] hydrogenase) is ligated to the protein moiety by a cysteine residue and the second atom is ligated by CO and CN.^{1,16,17,19-21} [Fe] hydrogenases possess only one iron atom and exert their catalytic function only in the presence of a second substrate (methenyl tetrahydromethanopterin).²² Ogata *et al.* obtained the crystal structure of [NiFe] hydrogenase from DvMF at 0.89 Å in 2015, which shed light on the structure of the intermediate state in the catalytic cycle.¹⁶ These studies reinforced the notion that the metals at the active site induce the heterolysis of molecular hydrogen. The present study used [NiFe] hydrogenase from DvMF because its high-resolution crystal structure and a large amount of spectroscopic data are available.^{9,15-17,20,21}

1-1-2 [NiFe] hydrogenase

[NiFe] hydrogenase consists of a large and a small subunit. A bimetal active site containing one Ni and one Fe is present in the large subunit and three iron-sulfur clusters are harbored in the small subunit. There are three important pathways in this enzyme: a gas transfer channel, a proton pathway, and an electron transfer pathway (Fig. 1-1). These pathways likely play crucial roles in controlling the physiological reaction catalyzed by hydrogenase.^{1,16} For example, the structures of these pathways may be key

factors for determining the O₂-sensitivity of [NiFe] hydrogenase.^{13,23,24} [FeFe] hydrogenase has a di-iron active site and also possesses these three pathways.¹⁹ The gas transfer pathway of [FeFe] hydrogenase is shorter than that of [NiFe] hydrogenase¹ and its turnover rate is higher than that of [NiFe] hydrogenase (Appendix I).^{8,9,12,25,26} The length or shape of the gas channel may regulate the properties (the rate and/or the direction of the physiological reaction) of each hydrogenase.^{1,13,23,27–29} Crystal structure analyses of hydrogenases show many hydrophobic cavities as candidate gas channels. However, there is no information on which cavity (or if all) is used and whether the shape dynamically changes during the reaction or not. Several candidate locations of proton pathways in [NiFe] hydrogenase have been proposed based on the results of crystal structure analysis and mutation experiments^{14,30}, but little is known regarding which are in fact used and how they are regulated during catalysis (e.g., whether the proton simply diffuses, or if there is a gate or another control mechanism). Fig. 1–2 shows one proposed catalytic mechanism for the reversible conversion of molecular hydrogen (H₂) to protons (H⁺) and electrons (e⁻), in which H₂ is heterolytically cleaved to produce hydride (H⁻) and proton (H⁺) when it binds to the Ni-SIa state. The hydride bridges the Ni and Fe and the proton is proposed to bind to the cysteine sulfur atom that coordinates the Ni. After releasing one proton and one electron, the Ni-R state transforms into the Ni-C state. After releasing one proton and one electron again, the Ni-C state returns to the Ni-SIa state. The reverse reaction is also believed to occur in the same manner. This proposed catalytic mechanism is based on high-resolution crystal structures and static spectroscopic data^{9,15–17,20,21} but the detailed conversion mechanism between each state remains unknown.

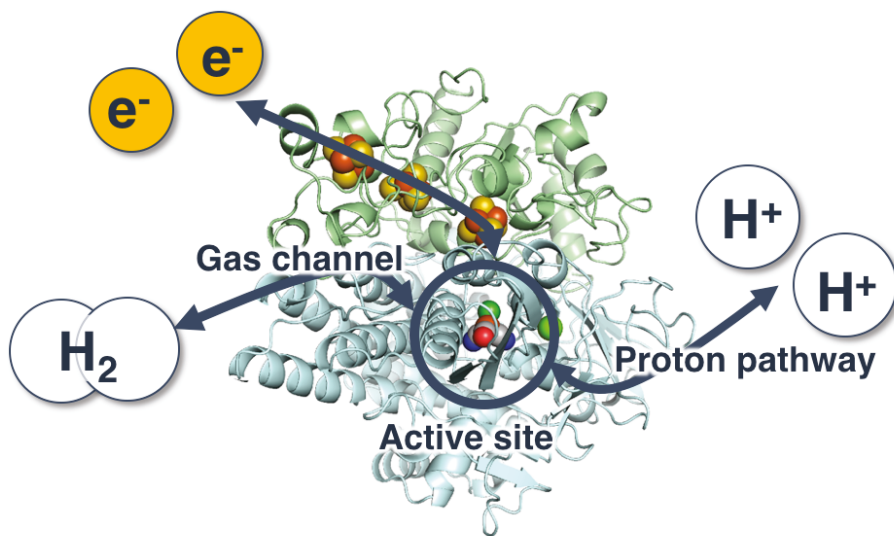


Figure 1–1. Crystal structure of [NiFe] hydrogenase from *Desulfovibrio vulgaris* Miyazaki F.¹⁶ [NiFe] hydrogenase possesses an electron transfer pathway (iron–sulfur cluster), a proton transfer pathway, and a gas channel, all located close to the active site.

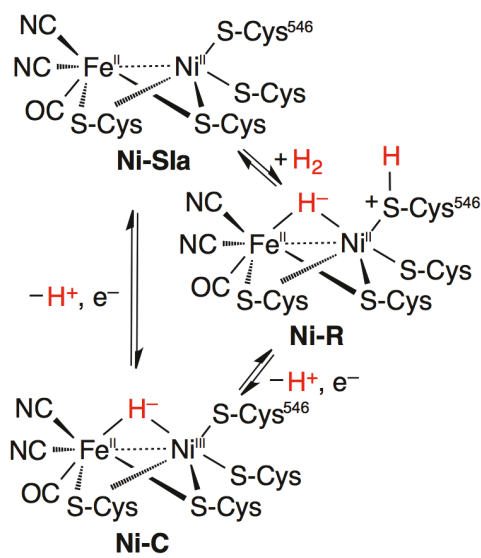


Figure 1–2. Proposed catalytic mechanism for the reversible oxidation of H₂ at the active site of [NiFe] hydrogenase.^{1,16,17,21}

The catalytic cycle consists of Ni-Sla, Ni-C and Ni-R states. The Ni-R state harbors a hydride bridge between the Ni and Fe, and the S of Cys546 is protonated.

1-1-3 H/D exchange and nuclear spin conversion reactions of hydrogenases

Hydrogen molecules, the substrate for hydrogenases, are so small that they cannot be either fluorescently labeled or structurally altered. Consequently, five isotopic and isomeric molecular hydrogen species (*para*-D₂, *ortho*-D₂, HD, *para*-H₂, and *ortho*-H₂) have been used to investigate hydrogenase-mediated reactions, in particular in two *in vitro* reactions: the H/D exchange reaction and the nuclear spin isomer conversion reaction. These reactions proceed without electron transfer to/from the mediators. In the H/D exchange reaction, the gaseous substrate is transferred via the gas channel to the active site, and then the covalent bond of H₂ is cleaved, followed by exchange between H⁺ and D⁺ (which requires the transfer of H⁺/D⁺ via the proton pathway) and subsequent re-formation of the bond at the active site. Molecular hydrogen can be either in the *para* or *ortho* state (details are given in Section 1-2-2). In the thermodynamic equilibrium state (also called the normal state), these two hydrogen states have a certain ratio. Under special conditions, the proportion of either state can be enriched^{31,32}. Either enriched state is not over a month to be transformed into the normal state without a catalyst.³² Hydrogenase can catalyze nuclear spin isomer conversion by cleaving the covalent bond of H₂. Hydrogenase-mediated conversion transfers the gaseous substrate via the gas channel, cleaves the H-H bond, and then re-forms the bond at the active site. The H/D exchange reaction and nuclear spin isomer conversion reaction were actively studied from the 1960s to the 1980s.^{4-6,9,11,12,33} Despite these efforts, no adequate data for kinetic analysis were obtained because the enzymes were not pure and appropriate methods for observing the time course of the reaction were lacking. Detailed investigation of the H/D exchange reaction, the nuclear spin isomer conversion reaction, and the combination of these reactions would provide insights into how the proton pathway and gas channel are

involved in the hydrogenase-mediated reaction. Current information on hydrogenases, including techniques for purification and mutation, are now much more advanced, allowing for more precise classical kinetic analysis of the H/D exchange and nuclear spin isomer conversion reactions. To this end, I have developed an assay method allowing detailed investigation of these two reactions easily and accurately (as described in Chapter 2).

[NiFe] hydrogenase from DvMF is easily inactivated under aerobic conditions. Hydrogenases used in previous studies of these reactions were aerobically purified. However, a recent study indicates that [NiFe] hydrogenase, once exposed to oxygen, does not completely return to its original structure even if reactivated.³⁴ I eliminated the influence of structural changes caused by oxygen by preparing hydrogenase anaerobically in this study. Furthermore, a small amount of methyl viologen or dithionite is typically added to the assay system to remove residual O₂.^{9,10,33} Electrons are not involved in either the H/D exchange or nuclear spin isomer conversion reactions. The addition of an electron mediator (such as methyl viologen) or a reductant (such as dithionite) results in a hydrogen production (or decomposition) reaction occurring simultaneously with the exchange or conversion reaction. Therefore, the exchange or conversion reaction was observed in isolation by conducting the experiments without adding either an electron mediator or a reducing agent. This makes it essential to optimize the experimental protocol for handling the purified hydrogenase under completely anaerobic conditions (as described in Chapter 3). Using the developed Raman system and the optimized experimental protocol, the H/D exchange reaction catalyzed by [NiFe] hydrogenase from DvMF was observed and kinetically analyzed (as described in Chapter 4).

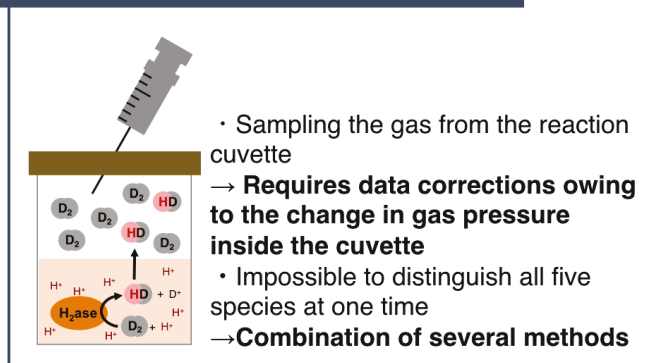
1-2 Raman spectroscopy

1-2-1 Comparison between Raman spectroscopy and other analytical methods

Absorption spectroscopy (ultraviolet-visible) and fluorescence spectroscopy are popular and easy methods for tracing enzymatic substrate conversion processes through continuous measurements. However, these methods are not applicable to all enzymatic reactions as the substrate and product must give different spectra. Gaseous molecules such as H₂ and D₂ do not absorb light in the visible region and are too small to be labeled with chromophores. Thus, the hydrogenase-mediated H/D exchange reaction is conventionally measured by gas chromatography (GC)⁹ and mass spectrometry (MS); indeed, most references cited in this thesis used MS for H/D exchange experiments. The nuclear spin isomer conversion reaction is generally measured by GC^{9,35} and thermal conductivity analysis^{4,36}. Details about these methods are summarized in the review by Vignais⁷ and in the book series 'Methods in Enzymology'.³⁷ Although these methods are well established, they require the use of cumbersome procedures to determine the composition of the gas phase in the reaction cuvette. More unfavorable, the gas must be extracted from the cuvette at regular intervals to monitor the reaction, resulting in changes in pressure of the gas phase after each sampling. In addition, several methods must be combined to observe the H/D exchange and nuclear spin isomer conversion reactions simultaneously, although sometimes this is impossible.^{9,35} Magnetic resonance methods, including NMR and EPR, and vibrational spectroscopy, including infrared (IR) and Raman spectroscopy, have emerged as candidate methods for monitoring the gas composition in the reaction cuvette continuously in a non-invasive manner. NMR and EPR detect species whose nuclei have nuclear spins and species with unpaired electrons, respectively. However, it is quite difficult to monitor gaseous samples by NMR due to

low sensitivity, and symmetrical diatomic molecules such as H₂ and D₂ cannot be detected by IR because this technique can detect only molecules whose dipole moment changes with molecular oscillation. In contrast, Raman spectroscopy can detect symmetrical diatomic molecules such as H₂ and D₂ because this technique can detect molecules whose polarizability changes with molecular oscillation. Fig. 1–3 conceptually illustrates the Raman measurement approach used in this study and compares the Raman method and conventional methods for tracing hydrogenase-mediated reactions by examining the temporal changes in the composition of the gas phase. Only the gas phase in the reaction cuvette is illuminated by the excitation light during Raman measurement and thus Raman spectroscopy is the most suitable method to observe the gas composition *in situ* without the need to extract sample material from the reaction cuvette. Raman spectroscopy allows the time course of the enzymatic activity to be traced without any data correction for changes in gas pressure inside the cuvette. Moreover, Raman spectroscopy has the additional advantage of permitting the continuous and simultaneous measurement of changes in the ratios of both isotopes and nuclear spin isomers.

Conventional methods:
gas chromatography(GC) and/or
mass spectrometry (MS)



In this study: Raman spectroscopy

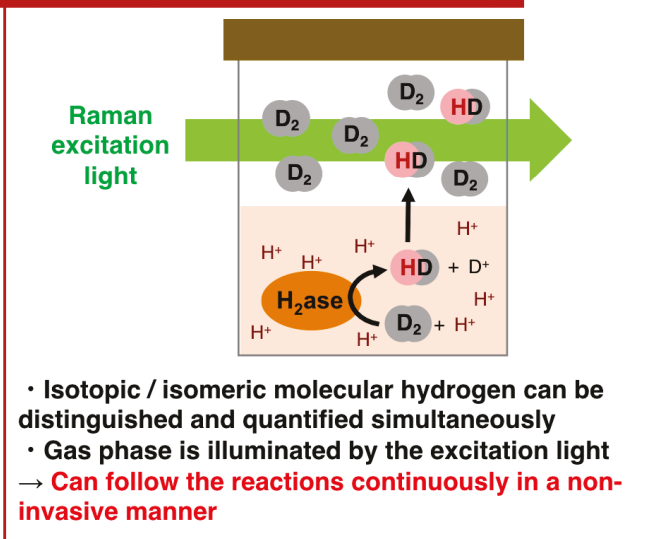


Figure 1–3. Comparison between conventional methods and Raman spectroscopy. Each method outlined is for an experiment tracing the H/D exchange reaction, where the gas phase is D_2 , the enzyme solution solvent is H_2O , and D_2 exchanges with H^+ in solution to produce HD or H_2 . These products are detected by extracting the gas sample from the reaction cuvette in the conventional method and by illuminating the gas phase with excitation light in the Raman method.

1-2-2 Raman spectroscopy for chemical analysis of reactions catalyzed by hydrogenase

Several principles of Raman spectroscopy are briefly introduced in this section to aid understanding of the Raman spectral analysis method described in Chapter 2. Irradiating a sample with light causes light scattering. Raman scattered light has wavelengths different from that of the incident light. The energy difference between the Raman scattered light and the incident (excitation) light corresponds to the vibrational (or rotational) energy in the molecule, and thus Raman spectra reflect the vibrational (or rotational) energy of the molecule in the sample. Isotopes can be distinguished by Raman spectroscopy since the vibrational energy of the molecule depends on the mass of the atom being probed. Nuclear spin isomers can also be distinguished by Raman spectroscopy. If symmetry is present in the molecular structure, the symmetry of the wave function is restricted by quantum statistics. For example, if the nucleus has a half integer spin in a symmetrical diatomic molecule (such as H₂), according to Fermi-Dirac statistics, the spin functions are singlet (antisymmetric, *para*) or triplet (symmetric, *ortho*) when the rotational quantum number (J) is even or odd, respectively. In the same manner, if the nucleus has an integer spin in a symmetrical diatomic molecule (such as D₂ and N₂), according to Bose-Einstein statistics, the spin functions are antisymmetric (*para*) or symmetric (*ortho*) when the rotational quantum number (J) is odd or even, respectively. Under ordinary conditions, the probability of changing the state of nuclear spin is very small, and thus *para*- and *ortho*-molecules behave as independent molecules³² and are called nuclear spin isomers. The Raman effect is observed only when $\Delta J = \pm 2$, according to the selection rules mentioned above. Thus, each Raman band observed in the rotational-vibrational Raman spectrum corresponds to one of the nuclear spin isomers,

allowing the five possible isotopic/isomeric species (*para*-D₂, *ortho*-D₂, HD, *para*-H₂, and *ortho*-H₂) to be distinguished by Raman spectroscopy in principle.

1-2-3 Shortcomings of Raman spectroscopy and strategies for overcoming them

Despite the enormous potential of Raman spectroscopy, to my knowledge there have been few reports of the application of this technique for monitoring enzymatic reactions³⁸ and no reports involving enzymatic reactions of gaseous substrates, likely reflecting several practical disadvantages of Raman spectroscopy. First, the substrate in the enzyme-substrate sample must be excited with intense laser light to obtain Raman spectra. The laser light potentially damages or inactivates the enzyme and thus preventing accurate measurements when the enzyme and the substrate are dissolved in the same solution. However, this drawback is prevented when the substrate is a gaseous molecule as only the gas phase in the reaction cuvette requires illumination with the excitation light. Second, Raman scattered light is very weak and thus readily overpowered by stray light, requiring long data collection times. Third, the absolute value of the concentration of the product cannot be obtained directly, as it can in absorption spectroscopy, since the Raman intensity varies depending on the specifications of the system and various parameters and measurement conditions.

In this study, I solved the above problems and developed a Raman spectroscopy-based assay system, as described in detail in Chapter 2.

Chapter 2

Development of a Raman Spectroscopy-based Assay System

2-1 Overview

As noted in Chapter 1, Raman spectroscopy has critical shortcomings for its application to the chemical analysis of hydrogenase-mediated reactions. The first, the weakness of the Raman signal, was solved by exhaustive optimization of the spectrometer and all optical elements. Noise sources such as stray light were removed as much as possible. The last problem, the difficulty of quantitative analysis of the absolute Raman intensity, was solved by using relative Raman intensity values calibrated using standard samples. Here, I provide a step-by-step description of the development of my Raman system and the method for analyzing the obtained data.

2-2 Development of the Raman system

2-2-1 Spectrometer, detector, and laser

Laser

Raman scattering was measured using a 532.0 nm Nd:YVO₄ laser (Millennia X, Spectra-Physics) as the excitation light source, with a power of 800 mW at the sample point. Non-resonance Raman spectra were observed in this study and thus the excitation light did not necessarily have to be 532.0 nm. Raman scattering is extremely weak under non-resonance conditions, requiring strong laser power. However, excessive laser power can be problematic, for example, generating strong stray light. Therefore, it is critically important to determine the optimal power of the laser light. The laser power of the excitation light must be at least 500 mW to obtain quality Raman spectra.

Spectrometer

A 30-cm spectrometer (Princeton Instruments Inc., Acton SpectraPro 300i) with a 500-nm blazed grating (1200 grooves/mm) was used in this study. The F-value of

the spectrometer was 4 and the central wavelength was set at 658 nm. It is essential to select an appropriate spectrometer and detector (groove frequency and detectable wavelength) according to the type of gas molecule to be observed, as the wavenumber region to be detected differs depending on the molecule. The present setup enabled me to conduct simultaneous measurements of a wide Raman spectral range (the wavelength range from around 2900 to 4200 cm^{-1} corresponding to 630 ~ 690 nm), including of D_2 , HD, and H_2 signals. The slit width was 50 μm , determined based on the quality of the Raman spectra as described in Section 2-2-4.

A view of the inside the spectrometer is shown in Fig. 2-1. First, the central wavelength was set to 532 nm. The light from the laser pointer (532 nm) was adjusted to pass through the approximate center of the entrance slit, all optical elements, and the CCD port in the spectrometer, and was used as a reference for alignment. It was essentially impossible for the light to pass through the exact center of all these components. For example, passage through the centers of the entrance slit, grating and CCD port caused the light to deviate greatly from the centers of the other mirrors. Consequently, the light was adjusted so that it strictly passed to the right of the middle of the entrance slit and the CCD port and deviations from the four optical elements became very similar. The height of the light from the bottom of the spectrometer was kept constant (within ± 1 mm), regardless of where it was measured in the spectrometer.

Detector

The detector was a liquid-nitrogen-cooled two-dimensional CCD (Roper Scientific Inc., Spec-10:400B) with the 1340 pixel detector array. CAUTION: the light from the laser pointer should NOT be introduced into the detector directly as this can seriously damage the device. The detector was attached to the spectrometer. Rough

alignments of detector for rotational angle and detector focus were performed using a fluorescent lamp. Fine alignment was conducted while measuring the Raman spectrum of the sample (H_2) to maximize resolution and intensity.

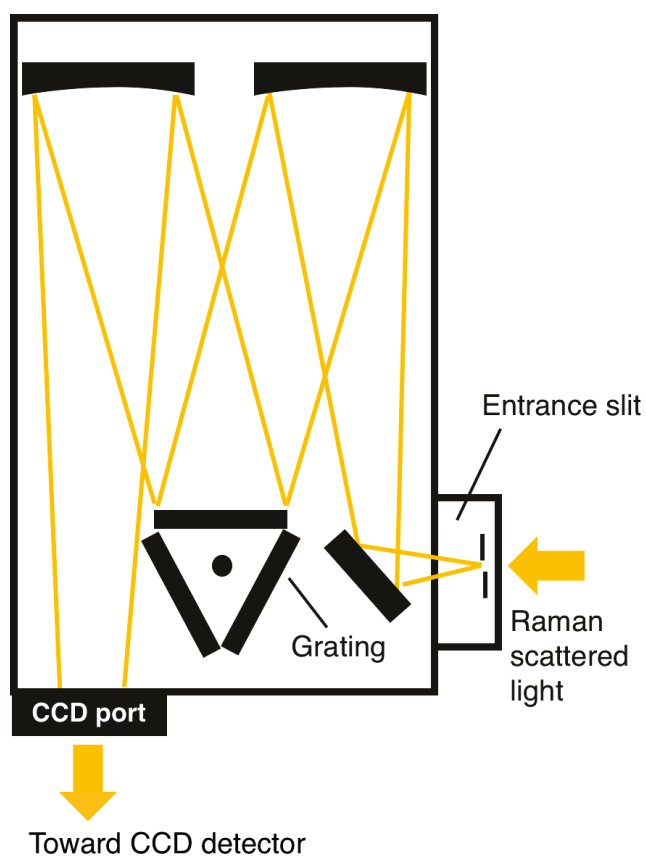


Figure 2–1. Plan view inside the spectrometer.

2-2-2 Alignment of the optical elements

All the optical components were installed on an optical table and arranged as shown in Fig. 2-2(A). This section describes the protocols essential for obtaining a high signal-to-noise ratio and high resolution.

Several mirrors (not shown in Fig. 2-2(A)) were placed in front of the laser oscillator so that the 532.0 nm laser (excitation) light was parallel to the optical table and intersected perpendicularly with the light from the laser pointer passing through the center of the spectrometer. This intersection point is the sample position. The mirrors were arranged so that the polarization plane of the laser light was parallel to the surface of the slit side of the spectrometer. The laser light was reflected vertically by each mirror. Lens-1 was placed so that the laser light was focused on the sample point. Two irises (not shown in Fig. 2-2(A)), lens-2, lens-3, and an edge filter were placed in front of the spectrometer so that the light from the laser pointer passed through their centers. Fine alignment of lens-2 and lens-3 was conducted while measuring Raman spectra of the sample (H_2) to maximize resolution and signal intensity. The F-value of the lens system used to collect the Raman scattered light (lens-2 and/or lens-3) was 11.2 and was determined based on the quality of the Raman spectra (resolution and signal intensity), as described in Section 2-2-4. The Raman system shown in Fig. 2-2(A) was placed in a metal framework completely covered with black cloth to isolate the system from stray light.

2-2-3 Thermostatically controlled cuvette holder

A water thermostatically controlled cuvette holder was placed at the sample position (Fig. 2-2(B)). The cuvette holder was maintained at the desired temperature by flowing water whose temperature was controlled by a thermostatically controlled

chamber connected via a copper pipe penetrating an aluminum plate. Heat diffusing toward the optical table decreased the efficiency of the temperature adjustment and thus an acrylic plate was sandwiched between the temperature control unit and the xyz axis translation stage to prevent this.

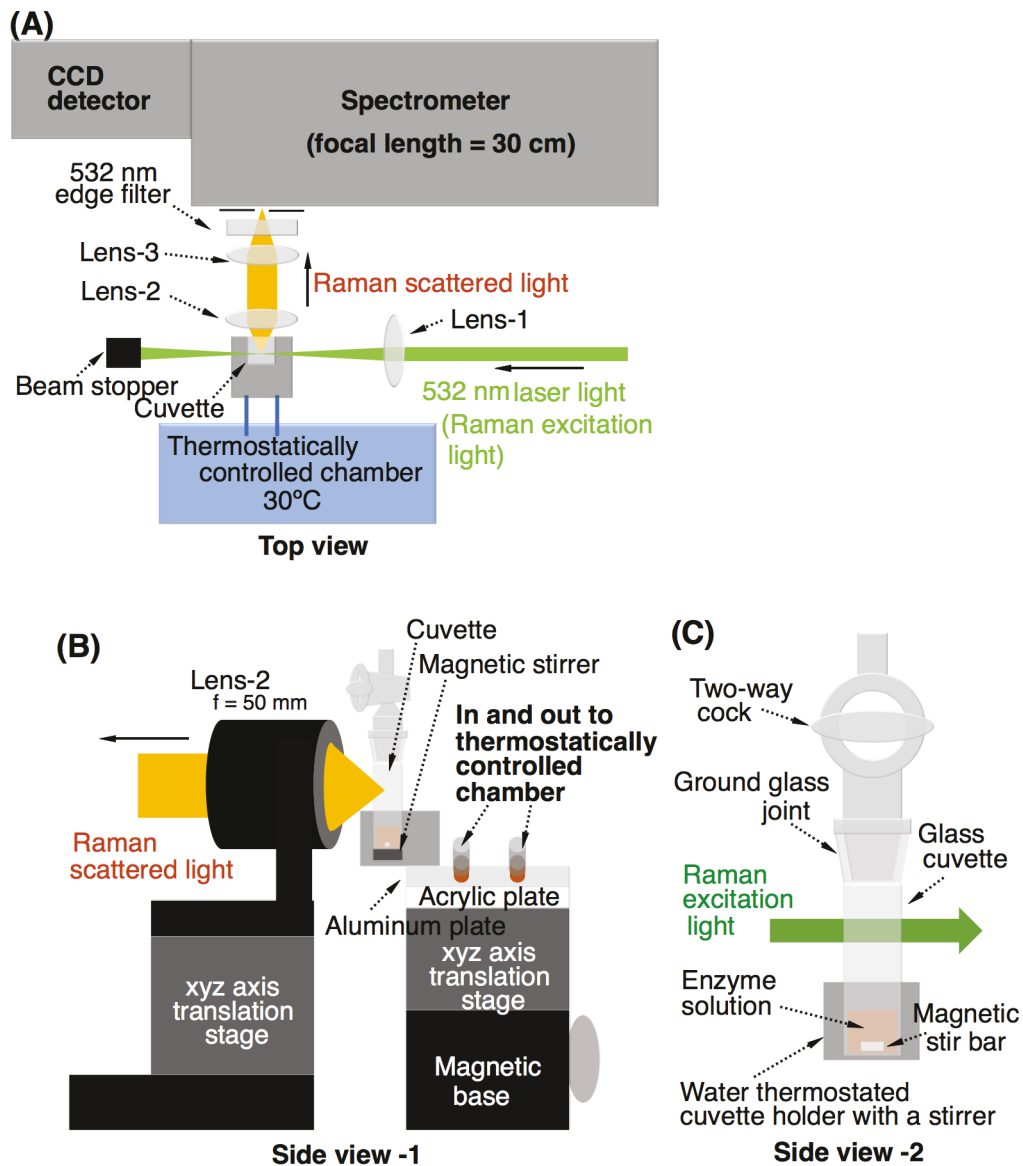


Figure 2–2. Experimental setup. (A) Schematic illustration of the Raman spectroscopy-based assay system. Lens-1: $f = 150$ mm, Lens-2: $f = 50$ mm, Lens-3: $f = 100$ mm (B) Schematic illustration of the water thermostatically controlled cuvette holder and the arrangement of the associated optical elements. (C) Custom-built reaction cuvette for anaerobic measurements of the reaction. The glass cuvette possesses four transparent surfaces for Raman measurements.

2–2–4 Fine alignment by optimizing the parameters and performance of the developed Raman system

First, fine alignment of the components was performed in the order detector, lens-1, lens-3 and lens-2 by filling a 10-mm glass cuvette (Fig. 2–2(C)) with four transparent sides containing indene and H₂ as standard reagents. Indene shows strong Raman scattering and H₂ is the substrate used for tracing the hydrogenase-mediated reaction. The resolution and intensity of the Raman spectra were essentially unaffected by the position of the focal point of the excitation light by lens-1 since the excitation light was perpendicular to the slit of the spectrometer. Lens-2 and lens-3 were carefully aligned so that the scattered light was focused on the center of the spectrometer slit.

As stated above, the F-value of the spectrometer used in this study was 4. Generally, it is better to match the F-value of the spectrometer and the lens system to collect the Raman scattered light (lens-2 and/or 3). A smaller F-value allows more light to be collected. However, if the diameter of the light beam entering the spectrometer is larger than the optical elements in the spectrometer, stray light will cause the baseline and noise to increase. Furthermore, light striking the edge of the optical elements in the spectrometer are affected by inherent aberrations of the optical elements, reducing the signal-to-noise ratio and resolution of the Raman spectra. On the other hand, if the diameter of the light beam entering the spectrometer is too small compared to the optical elements in the spectrometer, the diffraction efficiency of the grating decreases, reducing the intensity of the Raman spectra. Additionally, the larger the F-value, the less light can be collected, again decreasing the Raman intensity. When the F value of the lens system to collect the Raman scattered light (lens-2 and/or 3) was set to be much larger than the

F value of the spectrometer, a spectrum with the lowest amount of stray light (low baseline and high signal-to-noise ratio) and good sensitivity (high Raman intensity) was obtained, as shown in Fig. 2–3(A) and Table 2–I. The Raman spectra observed in this study were obtained using this alignment.

The slit width of the spectrometer is the most important parameter determining the resolution of the spectra. As shown in Fig. 2–3(B), when the slit width was too wide, the resolution decreased, whereas when it was too narrow, the Raman intensity decreased. Based on the Raman spectra shown in Fig. 2–3(B), the optimal slit width was determined to be 50 μm .

Even if the same alignment and sample are used, the Raman intensity will change by a maximum of 30% if the image location of the Raman scattered light on the detector changes (by changing the center wavelength of the spectrometer), as shown in Fig. 2–3(C). Hence, when the imaging position of the Raman scattered light on the detector changes greatly, the calibration described in section 2-3 must be performed again. Changing the center wavelength and then returning it to its original position shifted the imaging position of the peak maximum of the Raman band by 5 pixels while the shape of the Raman band did not change. Even if the center wavelength is not changed, the imaging position of the peak maximum of the Raman band varies by 1-2 pixels. Consequently, it is not possible to trace the changes in gas composition by using a Raman intensity at a fixed pixel.

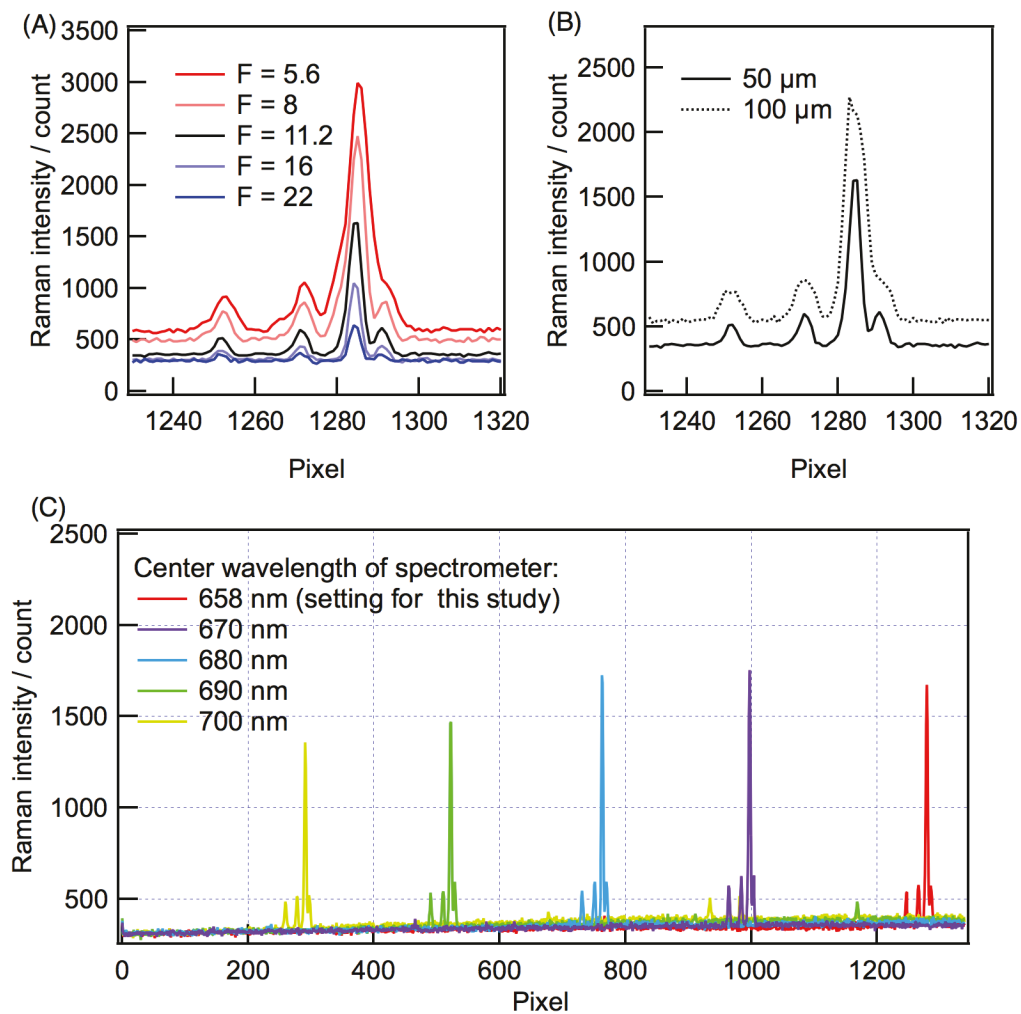


Figure 2–3. Rotational–vibrational spectra of pure H₂ measured using the Raman system. The exposure time was 60 s (no accumulation) for each spectrum. (A) and (B) show Raman spectra obtained with five F-values and two slit widths for the lens system used to collect the Raman scattered light, respectively. From these results, the slit width and F-value were set at 50 μm and 11.2, respectively. (C) Raman intensity change caused by changing the center wavelength of the spectrometer.

Table 2–I. Relationship between F-value and the Raman intensity, baseline, and signal-to-noise (S/N) ratio

F-value	Raman intensity at peak maximum / count	baseline / count	S/N ratio
5.6	2400	590 ± 30	80
8	1980	500 ± 30	70
11.2	1280	350 ± 10	128
16	740	310 ± 10	74
22	250	290 ± 10	25

2–3 Establishment of a quantitative analysis method for Raman spectra

Here I describe a method for quantitating the gas composition in the reaction cuvette using Raman spectroscopy. Such an analysis method is important for tracing the hydrogenase-mediated reaction accurately and analyzing the obtained data kinetically. As shown in the previous section, the absolute value of Raman intensity can change depending on measurement conditions, such as the imaging position of the Raman band on the detector. Therefore, the intensity ratio of pure gases (the substrate for hydrogenase) was measured under defined measurement conditions in advance, and relative values estimated from the intensity ratio were used in this analysis rather than the absolute values of the Raman intensities. Furthermore, it is not possible to trace the changes in sample composition by using a Raman intensity at a fixed pixel as discussed in the previous section. The relative values were therefore estimated from the area intensities of the Raman bands and not the Raman intensities at fixed pixels.

First, standard (pure) D₂, HD, and H₂ (1 atm) gases were measured using the developed Raman system (Fig. 2–4). The wavenumbers of D₂, HD, and H₂ have previously been reported, and highest peaks in the rotational–vibrational Raman spectra of D₂, HD, and H₂ are located at 2987, 3628, and 4155 cm⁻¹, respectively.³⁹ The wavenumbers in Fig. 2–4 were calibrated using these reported values.

Raman spectra for analysis were obtained by subtracting the blank spectrum obtained by measuring the reaction cuvette filled with air (N₂ and O₂ have no Raman bands in the wavelength range used for measuring D₂, HD, and H₂). Accurate ratios were obtained by measuring the Raman spectra of pure gases alternatively multiple times in one day. The area intensity of the Raman band of each isotope was calculated as follows. The X axes of the graphs used to calculate area intensities were pixels. Investigations of

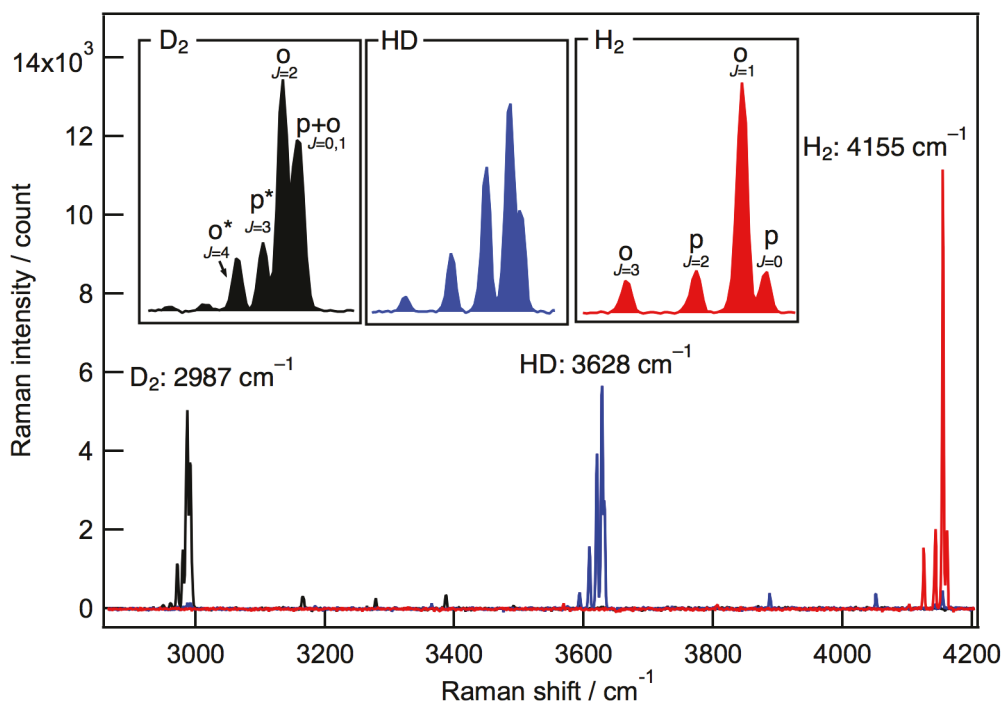


Figure 2–4. Rotational–vibrational spectra of gaseous molecular hydrogen species (H_2 , HD , and D_2) measured using the Raman spectroscopy-based assay system. The black, blue, and red lines represent the Raman spectra of D_2 , HD , and H_2 , respectively. The indicated wavenumbers are for the highest peaks of the individual isotopic hydrogen molecules. The upper three boxes show enlarged views of D_2 , HD , and H_2 . The characters *p* and *o* indicate the *para* and *ortho* states, respectively. The character *J* indicates the rotational quantum number. The Raman bands highlighted with asterisks were used for calculating the *para-ortho* ratio in D_2 . The area intensities of D_2 , HD , and H_2 were calculated from the area shaded in black, blue, and red, respectively.

time course changes in gas composition required removing spike noise as follows. A previous and a subsequent spectrum obtained after a given time were compared. If the Raman intensity at a particular pixel increased by more than a certain value (100 counts in the baseline region or 300 counts in the Raman band region for D₂, HD, and H₂), the Raman intensities of the spectra obtained before and after this spectrum were averaged to obtain the value for that pixel. The noise removal algorithm of the detector software cannot be used for this measurement since the Raman bandwidths of gaseous molecules are very narrow and thus the Raman band is erroneously recognized as spike noise. Assuming that the baseline is locally constant, the baseline was obtained by averaging the Raman intensities for 40 pixels just outside the region where the Raman band is observed. The area intensity of the Raman bands was calculated after subtracting the baseline from the Raman intensity. The area intensity of the Raman band was defined as the area delineated by the baseline and the Raman band, and was obtained by adding up all the Raman intensities in the region where the Raman band was observed. Trace amounts of D₂ and H₂ are present in commercially available HD and thus the area intensity of pure HD (1 atm) was estimated using the area intensities of pure D₂ and H₂. The D₂:HD:H₂ intensity ratio was 0.711(± 0.008):0.878 (± 0.011):1.

The molar fraction of each gaseous component was calculated using the following equations. The sensitivity of the detector was assumed to be linear in the range from 0 to 15000 counts.

$$\text{Molar fraction of D}_2 = (S_{D_2}/0.71)/(S_{D_2}/0.71 + S_{HD}/0.88 + S_{H_2}/1)$$

$$\text{Molar fraction of HD} = (S_{HD}/0.88)/(S_{D_2}/0.71 + S_{HD}/0.88 + S_{H_2}/1)$$

$$\text{Molar fraction of H}_2 = (S_{H_2}/1)/(S_{D_2}/0.71 + S_{HD}/0.88 + S_{H_2}/1)$$

where S_{D_2} , S_{HD} , and S_{H_2} are the area intensities of the Raman band for D_2 , HD, and H_2 , respectively, and the $D_2:HD:H_2$ intensity ratio was 0.71:0.88:1.

This Raman system allows the ratio of *para* and *ortho* states to be estimated. Since the Raman bands of *para*- H_2 and *ortho*- H_2 overlap each other, the area intensities of these bands must be obtained by fitting the Raman spectra to a sum of Gaussian functions (multi-peak fitting). The result of this fitting is shown in Fig. 2–5. H_2 in equilibrium at room temperature contains *para*- H_2 and *ortho*- H_2 in a ratio of 1:3 since H obeys Fermi-Dirac statistics. Consequently, the *para*- H_2 :*ortho*- H_2 area intensity ratio is 1:1.068 (± 0.010). Since some Raman bands of *para*- D_2 and *ortho*- D_2 overlap each other, I choose two Raman bands that are easy to distinguish for analyzing area intensities. These bands are marked with asterisks in Fig. 2–4 and are shaded blue for *para* and red for *ortho* in Fig. 2–5. D_2 in equilibrium at room temperature contains *para*- D_2 and *ortho*- D_2 in a ratio of 1:2 since D obeys Bose-Einstein statistics and thus the *para*- D_2 :*ortho*- D_2 area intensity ratio is 1:0.404 (± 0.008). Using these ratios together with the ratio for the isotopes estimated earlier, all five isotopic/isomeric species could be quantified.

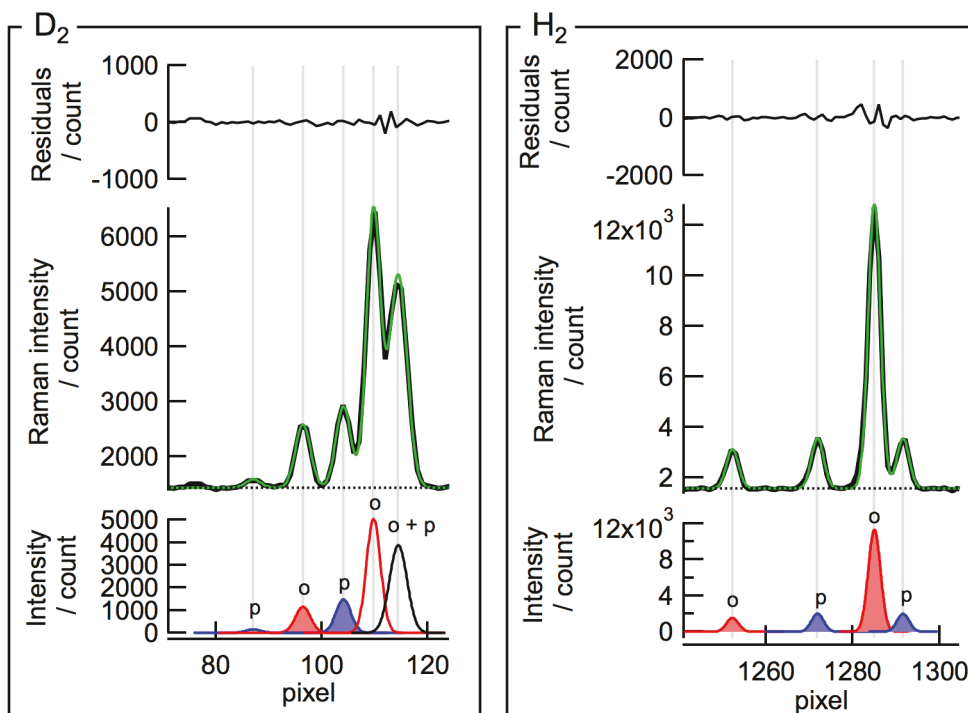


Figure 2–5. Results of multiplex fitting for the rotational–vibrational spectra of normal D_2 and H_2 . The upper, middle, and lower figures show the residuals in multiplex fitting, the fitting result, and the individual peaks in the fitting curve, respectively. The bold black lines represent the Raman spectra of D_2 or H_2 , and the green lines represent the multiplex fitting curves. The characters p and o indicate the *para* and *ortho* states, respectively. The area intensities of the filled peaks were used to calculate the ratio of the *para* and *ortho* states.

2-4 Summary

This chapter explained in detail the development of the Raman system and the quantitative analysis method for the Raman spectra. A schematic illustration of the developed Raman system is shown in Fig. 2-2. The specifications of the Raman system necessary for quantifying gas composition were first described, followed by the shape of thermostatically controlled cuvette holder (Fig. 2-2(B)). The most important factor for quantitatively analyzing temporal changes in gas composition is to obtain Raman spectra with high signal-to-noise ratio and high resolution with a short accumulation time. In particular, high resolution is required to distinguish and quantify nuclear spin isomers. In order to observe D₂, HD, and H₂ simultaneously, the wavelength range from around 2900 to 4200 cm⁻¹ (corresponding to 630 ~ 690 nm) must fit onto the 1340 pixels detector array. Obtaining high-resolution spectra that can distinguish rotational transitions required accurate alignment of all optical elements. This fine alignment was performed so as to maximize the resolution and signal intensity of Raman spectra for H₂ (Fig. 2-3(A) and (B)). As a result, Raman spectra with high signal-to-noise ratio and high resolution of D₂, HD, and H₂ were successfully obtained (Fig. 2-4). Furthermore, an analytical method for quantitatively calculating the gas composition of a sample from Raman spectra was established. Baseline estimation and spike noise removal methods were also developed. The Raman intensities of pure D₂, HD, and H₂ gases (the substrates and products of the hydrogenase-mediated reactions) were measured, and the area intensity ratio was experimentally obtained. Using this ratio, the ratio of the area intensity of the Raman band of each component during the reaction could be converted into the corresponding composition. Application of these methodological and analytical advances to the H/D exchange reaction catalyzed by hydrogenase provided the results described in Chapter 4.

Furthermore, although not described in this thesis, the nuclear spin conversion reaction can also be measured by using the ratio presented above.

Chapter 3

Optimization of Experimental Protocols

3-1 Overview

As mentioned in Chapter 1, [NiFe] hydrogenase from DvMF, which is the enzyme used in this study, is easily inactivated by oxygen contamination. It is common practice to add a small amount of reductant to remove residual O₂ from the enzyme solution^{9,10,33}, however, it may cause observation of a reaction different from the desired reaction. Therefore, the hydrogenase-mediated reaction assay was conducted without such a reductant. This makes it essential to handle the sample under strict anaerobic conditions at all stages of the experiment including the sample preparation, the initiation of the reaction, and the Raman measurement. The experimental protocol and the shape of the reaction cuvette were optimized to achieve strict anaerobic conditions. The optimization of the reaction cuvette was also important to obtain Raman spectrum with a flat baseline and control the contact interface between the enzyme solution and the gas phase. The optimization process of the reaction cuvette is summarized in Fig. 3-1. The a- and b-type of the reaction cuvette did not provide the reproducible result. By using these cuvettes, one of the following unfavorable phenomena was occurred: the reaction did not proceed, or the reaction ceased halfway, or the reaction rates did not reproduce even if the experiment was conducted under the same conditions. These failures have given me important information for considering experimental protocols. While referring to Fig. 3-1, I will discuss what was wrong in these methods and what was important in obtaining reproducible data. In the experiment, the enzyme solution and the substrate gas are brought into contact with each other in a reaction cuvette, and how the composition of the gas changes by enzymatic reaction is observed. The Raman part is already described in Chapter 2. Therefore, in this chapter, preparation of enzyme solution, substitution methods of gas phase and methods to initiate enzymatic reaction were

explained in this order followed by the explanation of the shape of reaction cuvette. Among the methods not used in this study, there are useful methods when designing other experiments. Methods that failed are also described in some detail. In this chapter, a protocol is explained by taking the H/D exchange reaction as an example, where the gas phase is D_2 , the solvent of the enzyme solution is H_2O , and D_2 exchanges with H^+ in solution to produce HD or H_2 (this measurement is called as H/D exchange reaction in D_2/H_2O system in this thesis). The result of tracing the H/D exchange reaction is analyzed in Chapter 4. The liquid phase, where the enzyme solution is poured, and the gas phase, initially filled with gaseous substrate, are marked with orange and green, respectively in Fig. 3-1.

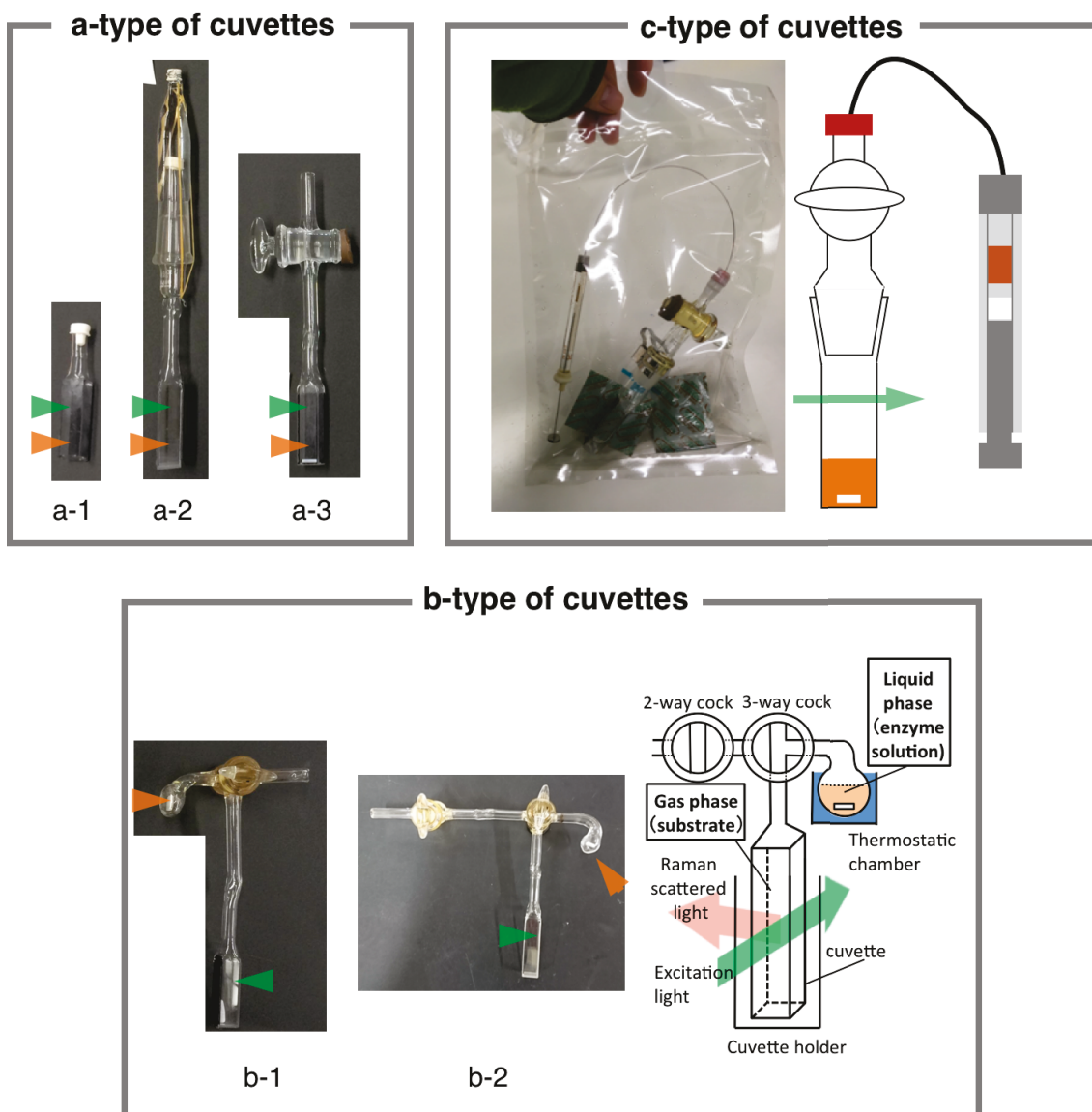


Figure 3–1. Custom-built reaction cuvettes explained in Chapter 3. The pictures of custom-built reaction cuvettes are shown in figure. The liquid phase, where the enzyme solution is poured, and the gas phase initially filled with gaseous substrates are marked with orange and green, respectively. Schematic illustration is shown for b-type of cuvette since the shape is complicated. The detail schematic illustration for c-type of cuvette is shown in Fig. 2–2(C). For c-type reaction cuvette, picture taken during the experiment and the schematic drawing of its setup are shown.

3-2 Optimization of experimental procedure

3-2-1 Shape of the custom-built reaction cuvette

While measuring the Raman spectrum, the dirt on the surface of the reaction cuvette causes a decrease in Raman intensity due to the blockage of the optical path for the excitation light and the Raman scattered light. In addition, the baseline of the Raman spectrum is disturbed by strong stray light scattered from the dirt. The precipitate of hydrogenase hardly dissolves in any of a detergent, a strong acid, and a strong alkaline solution. The easiest way to remove the precipitate sticking to the inner wall of the reaction cuvette is rubbing it with a cotton swab. However, the a-type of cuvettes, especially a-2 and a-3 do not allow the swab to reach the inner wall of optical surface. Changing the baseline significantly for each experiment, make it impossible to analyze the Raman spectrum properly, so this is a very simple but essential problem. The b-type of reaction cuvettes were developed to solve this problem. The gas phase part and the liquid phase part were connected each other with a three-way cock in this cuvette so that the enzyme solution did not touch the optical surface where lights pass. However, since the liquid phase part was handmade, the area of the gas-liquid interface could not be strictly controlled. Since the area of the gas-liquid interface determines the reaction rate of the enzymatic reaction (detail in Chapter 4), the individual difference of the reaction cuvette was reflected in the reaction rate, and the reaction rate could not be discussed quantitatively. Besides, it is impossible to examine the dependence of reaction rate on the volume of enzyme solution while keeping the surface area constant since the reservoir for the enzyme solution was spherical. this shape of cuvette in which the gas phase and liquid phase are connected with a cock makes it possible to use the best reaction initiation method when the glove box is far from Raman equipment as described in section 3-2-4

although they were not used in this study. Finally, c-type of reaction cuvettes were developed. In the cuvette, a two-way cock unit and a glass reaction cuvette are separated so that the optical surface can be cleaned easily by rubbing it with a cotton swab.

Regarding the shape of the reaction cuvette, preventing oxygen contamination while tracing the reaction is also important. Since the reaction time was very long (around a day), it was impossible to prevent oxygen contamination by closing the top of the branched reaction cuvette with a septum (Precision Seal Septa, sigma-aldrich) as a-1, or by placing a layer of water filled with nitrogen between the outside air and the entrance of the reaction cuvette as a-2. To prevent oxygen contamination, it was effective to close the glass cock which is sealed with high-vacuum sealant (Apiezon High Vacuum Sealants, M&I Materials Ltd.).

3-2-2 Preparation of the enzyme solution

[NiFe] hydrogenase from DvMF is easily inactivated by oxygen contamination. As a result of trial and error, the reproducible data could be obtained by performing all sample preparation procedure in a glove box (no more than 1 ppm). The glovebox (Coy Laboratory Products Inc.) was maintained under anoxic conditions with H₂ (1.5±0.5%) and N₂ (98.5±0.5%). Since the oxygen monitor in the glove box displays the oxygen concentration at one place in the glove, it does not guarantee the oxygen concentration in the whole part of the glove box (about 2 m³ of volume) is the indicated oxygen concentration. If the glove box contains only 1 ppm of oxygen, 1 ml of gas contains 4 nmol of oxygen molecules. The amount of hydrogenase molecule in 1 ml of 10 μM hydrogenase solution (typical measurement conditions in this study) is 10 nmol. Numerically, oxygen molecules contained in a few ml of gas in the glove box can

inactivate hydrogenases contained in 1ml of their solution. Therefore, the enzyme solution was quickly operated so as not to touch the gas in the glove box as much as possible. For the same reason, dissolved oxygen in the buffer solution was removed not by leaving the buffer solution in glove box, but by bubbling with argon gas for more than 1 hour prior to use in a glovebox. the argon gas was passed through ultrapure water prior to introducing the argon gas to the buffer solution to avoid changing the buffer concentration during the argon bubbling due to the vaporization of water in the buffer solution. The buffer solution was kept in a vial covered with butyl rubber stopper and aluminum flip off cap, and not opened in the glove box. The buffer was withdrawn by a syringe through the butyl rubber part when using it. [NiFe] hydrogenase from DvMF is inactivated relatively slowly under highly concentrated conditions compared to in diluted solution. This is presumably because the inactivated enzyme is auto-reactivated by other active enzymes using H₂ in the glove box. Therefore, the enzyme was stored at high concentration (~1.5 mM) in the glove box at 4°C. When storing the enzyme at a low concentration (~5 μM), the enzyme solution was stored in the vial covered with butyl rubber stopper and aluminum flip off cap and the gas phase in the vial was replaced with H₂.

The magnetic stirrer bar was evacuated for more than 30 minutes to completely remove oxygen adsorbed on the surface of the bar before using it for the measurement,. Similarly, syringes and tubes were evacuated before being placed in the glovebox or left there for 3 days or more. The high vacuum grease used to seal the glass cock was evacuated for 1 day before being placed in the glovebox and was left there for a week or more in the glove box since it absorbs oxygen inside a lot.

3–2–3 Substitution methods of the gas phase

The gas replacement system consists mainly of a vacuum pump, a gas cylinder and a joint part connecting them. Metal is better material for the joint part compared to rubber or plastic since a joint part made of metal can keep the inside under high vacuum and it does not absorb oxygen on the surface. However, the metal part could be a catalyst for *para* and *ortho* nuclear conversion reaction. It is inconvenient when measuring this reaction mediated by hydrogenase in the future. On the other hand, a joint part made of rubber or plastic easily absorb the oxygen on the surface. It is quite difficult to remove the oxygen completely and reproducibly. Moreover, the absorbed oxygen could be gradually exuded from the joint part during the operation of the gas replacement. The exuded oxygen possibly inactivates the oxygen-sensitive enzyme, which make it difficult to perform the reproducible experiment. Therefore, the substitution of the gas phase was performed in the glove box by using plastic and rubber tubes as the joint part so that the joint part neither become a catalyst for *para* and *ortho* nuclear conversion reaction nor is exposed to the air containing oxygen. A small vacuum pump, a small gas cylinder and the joint part were placed in the glove box. As described in section 3–2–2, it is unfavorable to expose the diluted hydrogenase solution to the atmospheres even in globe box. The inside of the gas replacement system was evacuated and replaced with the gas to be introduced (D_2 in this study) prior to the substitution of the gas phase in the reaction cuvette.

3–2–4 Methods to initiate enzymatic reactions

(I) *Adding the enzyme solution to the reaction cuvette with a syringe (for a- and c-type of cuvette)*

In this method, the enzyme solution is added to the reaction cuvette with a syringe to initiate the reaction. The advantage of this method is that the reaction can be started at the place where to measure Raman spectra (in the cuvette holder) rather than in the glove box so that the interval between the start time of the reaction and the start time of the measurement is short. This is especially useful when the glove box is far from Raman equipment. However, oxygen contamination during the operations of insertion and removal of a syringe causes the inactivation of the oxygen-sensitive enzyme. To avoid this, a layer of water filled with nitrogen was placed between the outside air and the entrance of the reaction cuvette as a-2. However, the water-layer method could not prevent the oxygen contamination through the cylinder part of the syringe. In fact, the phenomena that the reaction does not progress or stops halfway, which is probably caused by oxygen contamination, was observed. The following method make it possible to obtain the data with good reproducibility without being affected by oxygen.

A c-type of reaction cuvette was used for this method (diagram is shown in Fig. 2-2(C) and picture taken during the experiment is shown in Fig. 3-1 I). The reaction cuvette consisted of a glass reaction cuvette part and a two-way cock unit attached to the top of the cuvette via a ground glass joint. After connecting the two units at the ground glass joint with high-vacuum sealant, the gas inside the cuvette was replaced with D₂ gas at 100 kPa via a vacuum line connected to the inlet of the two-way cock unit. The two-way cock was closed prior to removal of the vacuum line. The inlet of the two-way cock was covered with a septum (Precision Seal Septa, sigma-aldrich). The hydrogenase solution was filled in a syringe and the needle of the syringe was stung into the septum. At this time, the two-way cock is kept closed. The syringe and the reaction cuvette are placed in a vacuum sealer bag (made of oxygen-impermeable material and generally used

for long-term storage of food) while the needle is kept stinging the septum. The top of the bag was closed with a sealer. A commercial oxygen scavenger and oxygen indicator (detection limit: 0.1%) was enclosed in the bag. All the operations so far were performed in the glove box. After bringing this outside the glove box and to the vicinity of the Raman equipment, a two-way cock was opened, the needle of the syringe was inserted to the bottom of the reaction cuvette, and the enzyme solution was gently placed in the reaction cuvette. After pouring the enzyme solution, the cylinder of the syringe was not let go of. After pulling up the needle tip of the syringe from the enzyme solution to the gas phase part of the reaction cuvette, the cylinder was released so that the pressure in the reaction cuvette became the same as the atmospheric pressure. After the needle was completely pulled out of the reaction cuvette. After the two-way cock was closed, the reaction cuvette was taken out from the bag. Finally, the reaction cuvette was placed in the cuvette holder in front of the spectrometer to initiate the Raman measurements. These procedures are too cumbersome but effective to prevent the oxygen contamination.

(II) Connecting a cock which separate the gas phase from the liquid phase (for b-type of cuvette)

In this method, the gas phase and the liquid phase are separated with a cock until a reaction is initiated by connecting a cock. This is the quickest way to initiate a reaction at the place where to measure Raman spectra (in the cuvette holder). This method can completely prevent the oxygen contamination. However, as described in section 3–2–1, it is difficult to control the surface area between liquid phase and gas phase. The experimental procedure is as follows. First, the three-way cock was turned in a direction that the reservoir part for the enzyme solution and the inlet of the cuvette were connected. The hydrogenase solution was placed in the reservoir part for the enzyme solution. Then,

the three-way cock was turned in a direction that gas phase and the inlet of the cuvette are connected prior to replacement of the atmosphere in the gas phase with D₂. The three-way cock was turned to a state where it was not connected anywhere. All the operations so far were performed in the glove box. Finally, the reaction cuvette was placed in the cuvette holder in front of the spectrometer to initiate the Raman measurements by connecting the gas phase with the liquid phase via three-way cock.

(III) Replacing gas in the gas phase with gaseous substrate (for a- and c-type of cuvette)

In this method, the reaction is initiated by replacing gas in the gas phase with gaseous substrate. The disadvantage of this method is that the reaction is initiated in the glove box and cannot be started where to measure Raman spectra (in the cuvette holder), so the interval between the start time of the reaction and the start time of the measurement is long (at least five minutes). It can be used when the glove box is close to Raman equipment. The merits of this method are that it can completely prevent the oxygen contamination and the operation is simple so that it is relatively easy to reproduce the result. In this study, this method is adopted. The detailed operation is described in the next section.

3-3 Optimized experimental methods for H/D exchange assay

A c-type of reaction cuvette was used for this method (Fig. 2-2(C)). The reaction cuvette consisted of a glass reaction cuvette and a two-way cock unit attached to the top of the cuvette via a ground glass joint part. The reaction cuvette and the magnetic stirrer bar were evacuated for more than 30 minutes to completely remove oxygen adsorbed on the surface of the bar by using oil-sealed rotary vacuum pump outside the glove box. Similarly, syringes and tubes were evacuated before being placed in the

glovebox or left there for 3 days or more. The reaction cuvette was placed in the glove box while kept vacuum. The hydrogenase solution was gently placed in the bottom of the reaction cuvette. The hydrogenase solution was prepared by diluting a concentrated stock solution with a buffer solution. Dissolved oxygen in the buffer solution was removed by bubbling with argon gas prior to use in a glovebox. The buffer solution was not opened in the glove box and was withdrawn by using a syringe. Details about the argon bubbling are described in section 3-2-2. The hydrogenase solution was quickly prepared so that the contact time with the atmosphere inside the glove box became as short as possible. After connecting the two units at the ground glass joint with high-vacuum sealant (Apiezon High Vacuum Sealants, M&I Materials Ltd.), the gas inside the cuvette was replaced with D₂ gas at 100 kPa via a vacuum line connected to the inlet of the two-way cock unit. The two-way cock was closed prior to removal of the vacuum line. Finally, the reaction cuvette was placed in the cuvette holder in front of the spectrometer to initiate the Raman measurements.

3-4 Summary and future perspectives

In this chapter, the optimization of experimental protocols was explained in detail. The most important topic was how to prevent oxygen contamination during the experimental operations. At first, the adequate shape of custom-built reaction cuvette for tracing H/D exchange reaction was discussed. The issues were the washing method inside the reaction cuvette, the reproducibility of the area of the gas-liquid interface, and the prevention of oxygen contamination during the measurement around for 1 day. The reaction cuvette that satisfies all these conditions was c-1 (Fig. 2-2 (C)) among those developed so far. All of the procedures except the Raman measurements were performed

in the glovebox. Even if the operation is performed in the glove box, there is a possibility that the enzyme is inactivated by residual oxygen. Therefore, when handling the enzyme solution in the glove box, the enzyme solution was quickly operated so as not to touch the gas in the glove box as much as possible. All the stuffs used for the preparation of enzyme solution (buffer solution, magnetic stirrer bar, etc.) were placed in the glove box after oxygen was removed in advance. There are three types of methods to initiate enzymatic reactions. In this chapter, the advantages and disadvantages of each method were discussed. Finally, the experimental protocols used in this study was summarized.

Although the hydrogenase-mediated reaction can be traced with good reproducibility by the above method, the problem remains. That is, it takes about one day for the reaction to progress by 90% since the amount of the substrate in the gas phase is too large with respect to the amount of enzyme (40 million times). Development of a reaction cuvette that reduces the volume of the gas phase and increases the area of the gas-liquid interface is desired to overcome this disadvantage (detailed reasons are shown in Chapter 4). Since measurement is conducted by warming the reaction cuvette to 30°C, if the gas-liquid interface is widened, the effect of volatilization of water from the enzyme solution will become unignorable. Development of a cuvette holder which can control the temperature of the whole reaction cuvette is also desired to prevent volatilization of water.

Chapter 4

Application of Raman-spectroscopy-based assay system to hydrogenase

4-1 Overview

As mentioned in Chapter 1, the substrate concentrations during the hydrogenase-mediated reaction can be estimated either directly by gas chromatography or mass spectrometry, or indirectly by absorption spectroscopy, if the catalytic reactions involve electron transfer with electron mediators that exhibit redox-dependent spectral changes.³⁷ However, these methods have critical shortcoming that the operation for measuring perturbs the reaction system such as pressure in the gas phase. In order to overcome the demerit, I have developed a new assay system for measuring the time course of enzymatic reactions involving gaseous substrates based on Raman spectroscopy. In Chapters 2 and 3 the development of Raman equipment and optimization of experimental operations were discussed. The developed system permits continuous monitoring of the gas composition in the reaction cuvette in a non-invasive manner over a prolonged time period. The additional advantage of the developed system is that it enables me to measure all of the hydrogenase-mediated reactions simultaneously. In this chapter, the developed system was applied to the kinetic study of the [NiFe] hydrogenase from *Desulfovibrio vulgaris* Miyazaki F.

4-2 Materials and methods

4-2-1 Materials and sample preparation

[NiFe] hydrogenase from DvMF was purified as described in the previous report.¹⁶ Enzyme purification was performed under strict anoxic conditions. The concentration of the hydrogenase was determined using the absorption coefficient at 400 nm ($47 \text{ mM}^{-1} \text{ cm}^{-1}$). H₂-uptake activity of the anaerobically purified enzyme assayed by the conventional spectroscopic method with methyl viologen was $5620 \text{ mol s}^{-1} (\text{mol}$

enzyme)⁻¹, which was a sufficiently high value compared to that (840 mol s⁻¹ (mol enzyme)⁻¹) prepared aerobically.¹⁷ The H/D exchange activities of [NiFe] hydrogenases were ranging from 45 to 450^{12,25}(summarized in appendix I), whereas that obtained using our system was 47 mol s⁻¹ (mol enzyme)⁻¹ at 20 nM. Although it is difficult to compare them directly due to the large differences of the experimental conditions, including the reaction cuvettes, bubbling conditions, additives (electron transfer media), the obtained value in this study was reasonable. The D₂/H⁺ exchange assay was performed in 25 mM Tris-HCl buffer (pH = 7.4). Dissolved oxygen in the buffer solution was removed by bubbling with argon gas prior to use in a glovebox. The glovebox (Coy Laboratory Products Inc.) was maintained under anoxic conditions with H₂ (1.5±0.5%) and N₂ (98.5±0.5%). H₂ gas (99.99%) was purchased from Taiyo Nippon Sanso Corporation. D₂ (99.8%) and HD (D: 97%) were purchased from Cambridge Isotope Laboratories Inc.

4-2-2 Raman spectroscopy (details in Chapter 2)

Raman scattering was measured using a 532.0 nm Nd:YVO₄ laser (Spectra-Physics, Millennia X) as the excitation source with a power of 800 mW at the sample point. The detector was a liquid-nitrogen-cooled CCD (Roper Scientific Inc., Spec-10:400B) attached to a 30-cm spectrometer (Princeton Instruments Inc., Acton SpectraPro 300i) with a 500-nm blazed grating with 1200 grooves/mm. This setup enabled us to carry out the simultaneous measurement of a wide Raman spectral range including the D₂, HD, and H₂ signals. The exposure time was 60 s and five scans were accumulated for each spectrum to provide a sufficiently high signal-to-noise ratio to allow quantitative discussion. The measurements were performed in a custom-built reaction cuvette as shown in Fig. 2-2(C). All of the optical components were installed on an

optical table and arranged as depicted in Fig. 2–2.

4–2–3 Assaying the H/D exchange reaction (details in Chapter 3)

The reaction vessel consisted of a glass reaction cuvette and a two-way cock unit attached to the top of the cuvette via a ground glass joint. The hydrogenase solution was placed in the reaction cuvette. After connecting the two units at the ground glass joint, the gas inside the cuvette was replaced with D₂ gas at 100 kPa via a vacuum line connected. The two-way cock was closed prior to removal of the vacuum line. Finally, the reaction cuvette was placed in the cuvette holder in front of the spectrometer to initiate the Raman measurements. The reaction mixture was continuously stirred (1000 rpm) using a magnetic stirrer and maintained at 30°C in a thermostatically controlled chamber (Fig. 2–2(B)). Unless otherwise noted, the volumes of the reaction mixture and gas phase were 1 mL and 10 mL, respectively. Since the droplets attached on the wall of the inside of the cuvette by the splashed solution of the reaction mixture disturb the transmission of the laser light, resulting in the inaccurate measurement of the Raman peak intensity, the enzyme solution was not able to be stirred vigorously in the present measurement system. This could be solved by improving the reaction system in future work. All of the procedures except the Raman measurements were performed in the glovebox.

4–2–4 Data analysis

The area intensities of the Raman bands for each pure isotope individually were measured. The D₂:HD:H₂ intensity ratio was 0.71:0.88:1. The observed area intensities of the Raman bands of the individual isotopic species were corrected by dividing by these values to obtain the molar fraction of each isotopic species (details in Chapter 2).

The fractions of the isotopic species in the period from the start of the measurement to half of the half-life of D₂ were used to calculate the initial rates of HD and H₂ production. The data were least-squares fitted with a straight line to obtain the slopes corresponding to v_1 and v_2 for HD and H₂, respectively.

The time courses of the D₂/H⁺ exchange reactions were fitted using the analytical solution of the reaction model depicted in Fig. 4–1. The calculations were reported by Leroux *et al.*¹³ The initial conditions were [D₂]₀ = 1, [HD]₀ = 0, and [H₂]₀ = 0. The equations used for the fitting were as follows:

$$[D_2] = [D_2]_0 e^{-[k_a / (1+kb)] t}$$

$$[HD] = 2[D_2]_0 \{e^{-[k_a / (2+kb)] t} - e^{-[k_a / (1+kb)] t}\}$$

$$[H_2] = [D_2]_0 (1 - 2e^{-[k_a / (2+kb)] t} + e^{-[k_a / (1+kb)] t})$$

where $k_a = (k \times k_{in} \times [E]_0) / (k_{out} + k_{in} \times [D_2]_0)$, $k_b = k / k_{out}$, and [E]₀ is the enzyme concentration. The other terms are explained in the Results section and Fig. 4–1. The fitting was performed using built in macro for global fitting in a software of Igor pro (ver. 6) provided by WaveMetrics. In fitting, it was assumed that the parameters k_a and k_b are common to all the time courses of D₂, HD, and H₂ obtained by a single measurement.

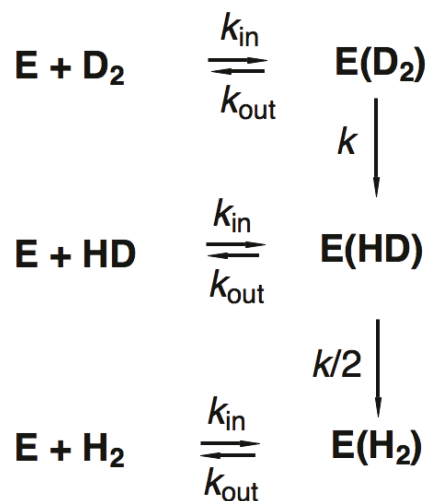


Figure 4–1. Scheme of the H/D exchange reaction used for the kinetic analysis.¹³ E represents the free enzyme, and E(D₂), E(HD), and E(H₂) represent the enzyme bound to D₂, HD, and H₂, respectively. The rate constant from E(HD) to E(H₂) is not *k* but *k*/2 since E(HD) is ready to become E(H₂) only when HD is dissociated into H⁻ and D⁺ (not D⁻ and H⁺).

4-3 Results

4-3-1 Continuous monitoring of the catalytic reaction by Raman spectroscopy

In the system shown in Fig. 2-2, only the gas phase in the reaction cuvette is illuminated by the excitation light, such that the enzyme in the solution phase is not damaged or otherwise affected. Since there is no need to withdraw aliquots of gas from the reaction cuvette to measure the Raman spectra, the reaction conditions such as pressure and temperature can be kept constant. In fact, Raman intensity of D₂/H₂ (1 atm) in the reaction cuvette did not change at all for over one day. It is common practice to add a small amount of dithionite to remove residual O₂ from the assay system of hydrogenases.^{9,10,33} In this study, however, the reaction mixture was anaerobically prepared in the custom-built reaction cuvette shown in Fig. 2-2(C) inside a glovebox and no reductants are required (see Materials and methods and Chapter 3). The highest peaks in the rotational-vibrational Raman spectrum of D₂, HD, and H₂ locates at 2987, 3628, and 4155 cm⁻¹, respectively, as shown in Fig. 2-4.³⁹ All of the peaks originating from the sample gases were observed simultaneously in a single spectrum. The resolution of the system was sufficient for discrimination of the rotational states (spin isomers); five peaks corresponding to the possible isotopic/isomeric species (*para*-D₂, *ortho*-D₂, HD, *para*-H₂, and *ortho*-H₂) could be clearly distinguished as labeled in Fig. 2-4 (see Chapter 2).

4-3-2 H/D exchange reaction in the D₂/H₂O system

Fig. 4-2(A) shows the time course of the Raman peak intensities of D₂, HD, and H₂ during the H/D exchange reaction in the D₂/H₂O system catalyzed by the [NiFe] hydrogenase from DvMF (10 μM) at 30°C. During the course of the reaction, the Raman peak intensities of D₂ and H₂ exhibited a simple decay and rise, respectively. In contrast,

the Raman peak intensity of HD increased over the period from 0 to 200 min, began to decay after 200 min, and then finally disappeared at 1000 min. The amounts of D₂, HD, and H₂ were estimated by calculating the area intensities of the corresponding Raman bands, which were normalized using standard gases (see Materials and methods and Chapter 2). Since the total number of gas molecules in the reaction cuvette during the H/D exchange reaction was kept unchanged, each of the gaseous components is hereafter represented as a molar fraction. As shown in Fig. 4–2(B), the time course data obtained for the H/D exchange reaction were sufficiently accurate to permit precise evaluation of the kinetics of our system.

The time course of the D₂ fraction revealed that this component underwent exponential decay, where the time constant (pseudo–first-order rate constant) (τ_D) at the enzyme concentration of 10 μM was $0.0050 \pm 0.0004 \text{ min}^{-1}$. The dependency of enzyme concentration was observed in τ_D at the range of 2 – 20 μM in Fig. 4–3. Since no accelerated features were observed on the H/D exchange reaction at the initial stage of the reactions (Fig. 4–2(B)), the enzyme samples used in this study have a full activity from the beginning of the measurements.

In the developed system, the reaction mixture could not be stirred vigorously (see Materials and methods). In addition, this measurement setup resulted in the large volume of the gas phase compared to the liquid phase. For these reasons, we had to use the concentrated enzyme solutions (2, 5, 10 and 20 μM) to measure the time course of the H/D exchange reaction in an appropriate period of time. The H/D exchange activities (2 – 6 mol (D₂) s⁻¹ (mol enzyme)⁻¹) calculated from the initial rates of D₂ consumption for the concentrated enzyme solutions (Table 4–I) were considerably lower than those estimated from the previous reports^{9,17} (about 120 mol s⁻¹ (mol enzyme)⁻¹). Since the

dependency of the H/D exchange activity on the enzyme concentration was reported before,⁹ experiments with the diluted enzyme solutions were carried out. The activity estimated from 20 nM enzyme showed comparable value ($47 \text{ mol s}^{-1} (\text{mol enzyme})^{-1}$) as shown in Table 4-I, if the large differences of the experimental conditions between two methods are taken into account (see Materials and methods). In order to investigate the characteristics of the reaction system, τ_D at various volumes of enzyme solutions were calculated (Table 4-II).

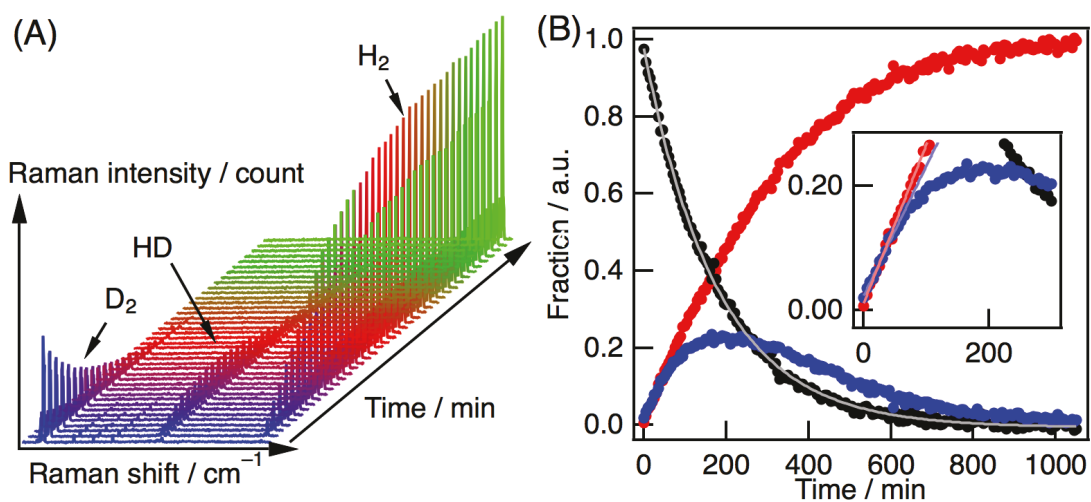


Figure 4–2. H/D exchange reaction in the D₂/H₂O system catalyzed by [NiFe] hydrogenase from *Desulfovibrio vulgaris* Miyazaki F. (A) Waterfall plot of the Raman spectra obtained at 25-min intervals during the H/D exchange reaction in the D₂/H₂O system. (B) Time course of the isotopic composition of molecular hydrogen. The black, blue, and red markers represent the fractions of D₂, HD, and H₂, respectively. The gray line over the black markers represents the fitting curve for the exponential decay of D₂. The pale blue and pale red lines in the inset represent the fitting curves for the initial reaction rates of HD and H₂ production, respectively.

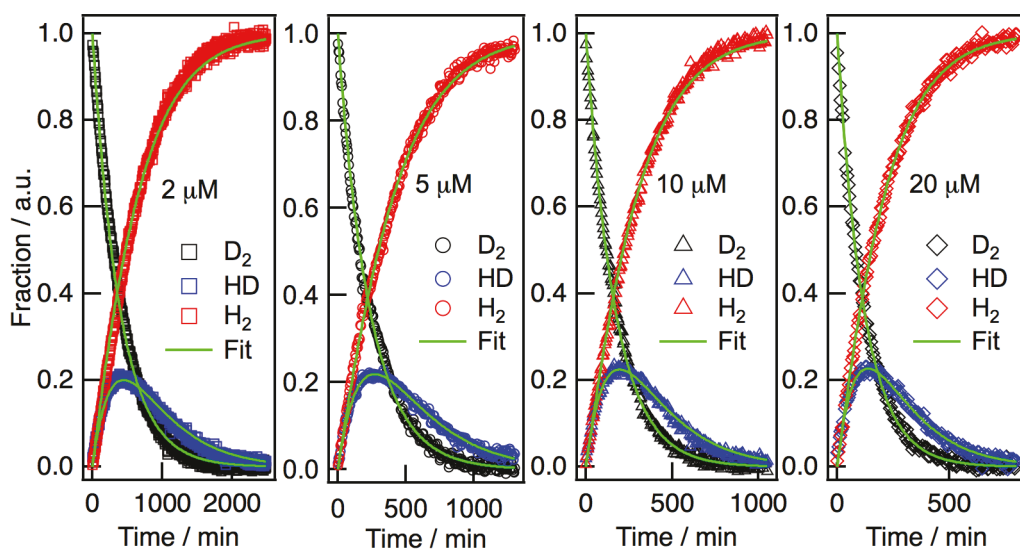


Figure 4–3. Kinetic analysis of the time course of the H/D exchange reaction catalyzed by [NiFe] hydrogenase. The time course of the reaction was measured at enzyme concentrations of 2, 5, 10, and 20 μM . The black, blue, and red markers represent the molar fractions of D₂, HD, and H₂, respectively. The green lines over the markers represent the fitting curves calculated using the equations based on the model depicted in Fig. 4–1. The interval between each measurement was 5 min.

Table 4–I. H/D exchange activities for several enzyme concentrations

Enzyme / μM	H/D exchange activity / mol (D ₂) s ⁻¹ (mol enzyme) ⁻¹
0.02	47 ± 5
0.2	15 ± 4
2	5.9 ± 0.8
5	4.2 ± 0.5
10	2.7 ± 0.3
20	2.0 ± 0.3

Table 4–II. τ_D for several volumes of reaction mixture at 10 μM enzyme concentration

Volume / μL	τ_D / min ⁻¹
250	0.0041 ± 0.0001
500	0.0041 ± 0.0006
1000	0.0050 ± 0.0004

*normalized data based on the volume of gas phase

The initial production rate of HD (v_1 , $0.0018 \pm 0.0002 \text{ min}^{-1}$ at the enzyme concentration of $10 \text{ }\mu\text{M}$) was almost equal to that of H_2 (v_2 , $0.0022 \pm 0.0003 \text{ min}^{-1}$). These results could not be adequately analyzed using the simple stepwise reaction mechanism shown in equations 1 and 2, indicating that not only the single exchange reactions (e.g., $\text{D}_2 + \text{H}^+ \rightarrow \text{HD} + \text{D}^+$) but also the double exchange reaction (i.e., $\text{D}_2 + 2\text{H}^+ \rightarrow \text{H}_2 + 2\text{D}^+$) occurred macroscopically in the reaction cuvette.



4-3-3 Effect of the product release rate from the hydrogenase in the H/D exchange reaction using a kinetic model

To analyze the time course of the H/D exchange reaction in the $\text{D}_2/\text{H}_2\text{O}$ system quantitatively, the reaction model proposed by Leroux *et al.*, as depicted in Fig. 4-1¹³ was adopted. In this model, k is the rate constant of the H/D exchange reaction at the active site and k_{in} and k_{out} are the rate constants for the trapping and release, respectively, of molecular hydrogen species by the hydrogenase molecule. To obtain the ratios of k to k_{out} , the time courses of D_2 , HD and H_2 at several enzyme concentrations were fitted against the analytical solutions derived from the model equations presented in Fig. 4-1. As indicated by the green lines in Fig. 4-3, the fitted curves were in good agreement with the experimental data. The values of k/k_{out} (1.8-2.1) were approximately constant for enzyme concentrations in the range of 2-20 μM (Table 4-III), and similar to those calculated by the method where the maximum points of HD are used.¹³

Table 4–III. τ_D , v_2/v_1 , k_a and k_b for several enzyme concentrations

Enzyme / μM	τ_D / min^{-1}	v_2/v_1	k_a	k_b
2	0.0022 ± 0.0003	1.34 ± 0.08	0.007 ± 0.001	2.14 ± 0.18
5	0.0038 ± 0.0003	1.20 ± 0.05	0.011 ± 0.001	1.86 ± 0.02
10	0.0050 ± 0.0004	1.22 ± 0.07	0.015 ± 0.001	1.83 ± 0.03
20	0.0074 ± 0.0010	1.18 ± 0.06	0.016 ± 0.003	1.83 ± 0.04

All data are the average results obtained from three independently purified enzyme solutions.

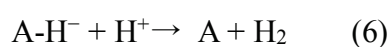
$$k_a = (k \times k_{\text{in}} \times [\text{E}]_0) / (k_{\text{out}} + k_{\text{in}} \times [\text{D}_2]_0)$$

$$k_b = k / k_{\text{out}}$$

4-4 Discussion

Until the 1990s, H/D exchange reactions by hydrogenases were studied and discussed with respect to the initial reaction rates of HD and H₂ production, where the main focus was the mechanism of the double exchange reaction.^{4-7,9,11,13,25,35} Recently, the technique of online mass spectrometry^{40,41}, which allows monitoring of the time course of the variation of the gas composition of the reaction, has been used to obtain more detailed information regarding the mechanism of the H/D exchange reaction.^{13,42} However, it is difficult to survey the entire time course of the reaction by mass spectrometry owing to the continuous consumption of the gas in the reaction cuvette during sampling. Using the newly developed system based on Raman spectroscopy, we confirmed that H₂ (i.e., the fully exchanged product) is concomitantly produced alongside HD during the H/D exchange reaction in the D₂/H₂O system. As shown in Fig. 4-2(B), the initial production rates of HD and H₂ were almost equal.

It is generally accepted that D₂ is heterolytically cleaved to produce D⁻ and D⁺ following binding to the Ni-Fe active site. The D⁻ bridges the Ni and Fe and the D⁺ is proposed to bind to the cysteine (Cys546) sulfur atom that coordinates the Ni (the Ni-R state in Fig. 1-2).^{1,16,17,21} In the D₂/H₂O system, the formation of HD and H₂ at the Ni-Fe active site is supposed to proceed according to equations 3 – 6:



where “A” and “A-H⁻ + H⁺” represent the Ni-Fe active site and the Ni-R state,

respectively, as shown in Fig. 1–2. According to equations 3 – 6, H₂ should appear after HD production. In the D₂/H₂O system, the fully exchanged product (H₂) could be produced by two successive single H/D exchange reactions (1) in different active sites or (2) at the same active site (macroscopically double exchange reaction).^{5–7,9–11,13} Since the ratio of v_2/v_1 depended little on the enzyme concentrations (Table 4–III), the former is denied. Besides, τ_D depended on the enzyme concentration and did not depend on the volume of the enzyme solution. The results indicate that the reaction probably occurred near the gas-liquid interface and not controlled by the diffusion of the substrate. Hence, the entire time courses of individual components in the reaction were quantitatively analyzed and well fitted to the equations derived from the previously described reaction model (Fig. 4–1).¹³ From the fitting results in Fig. 4–3, k/k_{out} was estimated to be 1.9 ± 0.2 (Table 4–III). This obtained value indicates that the rates of the H/D exchange reaction at the active site and the release of the products from the enzyme were comparable. Hamdan *et al.*, reported that k and k_{out} can be separately calculated under the condition of largely excess concentration of substrate over Michaelis constant, K_m .²⁹ Although k/k_{out} was successfully estimated in this study, it is difficult to apply this approximation because there is insufficient substrate concentration in the solution (760 μ M) against K_m of DvMF (130 μ M for D₂ in the H/D exchange reaction)⁹ and to discuss the relationship between k_{in} and k_{out} based on the present reaction model.

In the experimental setup of our Raman system using concentrated enzyme solution, the enzymatic reaction mainly takes place at the interface between the gas and liquid phases. This is one of the reasons that the activities of the H/D exchange reaction showed the dependency of the enzyme concentrations (Table 4–I). Nevertheless, τ_D of D₂ decay with the concentrated enzyme in this study was dependent on the enzyme concentrations

(probably on the enzyme density at the interface) and k/k_{out} was successfully estimated from the entire time course of the H/D exchange reaction. These results indicate that the data obtained in this study were not controlled by the diffusion limit of the substrate at the liquid-gas interface, but demonstrated the typical feature of the enzymatic reaction, even though the improvement of the measurement system is required for further assay of the H/D exchange activity of the enzyme more accurately.

Chapter 5

Conclusion and Future Perspectives

Hydrogen is the simplest and the lightest of the elements. Conversion of the chemical energy in molecular hydrogen into electrical energy produces water as the only by-product. Liquid hydrogen fuel has the highest energy density per unit mass of all conventional fuels. Based on these beneficial features, hydrogen has attracted attention as an ideal energy carrier. In order to realize a society that uses hydrogen as an energy carrier, a number of technical problems must be solved: (1) the production of hydrogen from renewable energy sources such as wind and solar power, (2) efficient storage and transportation systems for the synthesized hydrogen, and (3) efficient and safe *in situ* use of hydrogen energy.⁴³ Hydrogenases efficiently catalyze the reversible conversion of molecular hydrogen (H_2) to protons (H^+) and electrons (e^-) under mild conditions. Methods using hydrogenase as a synthesis catalyst for hydrogen production^{17,44} and an electrode catalyst for a fuel cell⁴⁵ have been studied. Understanding the underlying catalytic mechanisms is desirable for developing more active and inexpensive catalysts and may even lead to the discovery of new chemical phenomena.⁴⁶

From an academic perspective, hydrogenase is a very interesting enzyme because it possesses a gas channel (the substrate transport pathway), a proton pathway, and an electron transfer pathway. Analysis of the hydrogenase crystal structure has identified many candidate gas channels and proton pathways.^{23,27,28,30} However, there is little information regarding how these pathways dynamically work at the atomic level and cooperate during the reaction at the active site. To answer the question, the kinetics of the H/D exchange reaction and nuclear spin isomer conversion reaction has been investigated.^{13,14,29} Unfortunately, the conventional methods used to study these reactions has critical shortcomings, such as requiring extraction of gas samples from the cuvette at regular intervals to monitor the reaction, thereby changing the pressure of the gas phase

after sampling.

To address these shortcomings, I developed a new Raman spectroscopy-based assay system specifically to trace enzymatic reactions. Raman spectroscopy allows direct observation of the vibrational and rotational transitions of molecules. These transitions are specific for each type of molecule. Consequently, the gas composition in the reaction cuvette can be estimated continuously by simply illuminating the gas phase sample with excitation light. After overcoming some challenges particular to the Raman method, the resolution and signal-to-noise ratio of the Raman spectra acquired by the system enabled the discrimination and quantification of isotopes and nuclear spin isomers. A method for quantitatively analyzing Raman spectra was also established. Using this system, the H/D exchange reaction catalyzed by [NiFe] hydrogenase from DvMF was traced by continuous monitoring of the gas composition in the reaction cuvette in a non-invasive manner over a prolonged time period. The time course data for the reaction were sufficiently accurate to be kinetically analyzed in detail. To obtain reproducible results, it was necessary to devise protocols for handling the samples. For example, oxygen contamination was the most significant factor reducing reproducibility and thus all experimental operations were conducted in a glovebox except for the Raman measurements. Oxygen was removed from all equipment and materials prior to bringing them into the glovebox. The diluted hydrogenase solution was kept sealed in the glovebox.

Fitting the obtained data to the kinetic model revealed that the rates of the H/D exchange reaction at the active site and the release of the products from the enzyme were comparable. However, the assumption that all molecular hydrogen species share the same kinetics in the reaction model used in this study is not necessarily valid, because the

masses of D₂ and HD are respectively 2-fold and 1.5-fold the mass of H₂, while the kinetic isotope effect is probably as high as 17-fold and 4-fold that of H₂, respectively. Unfortunately, my investigation of the H/D exchange reaction in a D₂/H₂O system did not provide information on the function of the proton pathway and will require investigation of the following reactions: (1) the H/D exchange reaction in an H₂/D₂O system; and (2) the nuclear spin isomer conversion reaction, that is, the conversion between *para*-H₂ and *ortho*-H₂ (or between *ortho*-D₂ and *para*-D₂) in H₂O or D₂O. These measurements can be performed using the same assay system described in Chapter 2.

Representative examples of enzymes catalyzing reactions of gaseous molecules other than hydrogenase are cytochrome c oxidase (O₂)⁴⁷, nitrogenase (N₂)⁴⁸, NO reductase (NO and N₂O)⁴⁹, and methane monooxygenase (CH₄ and O₂)⁵⁰, all of which play crucial roles in biological systems. Electrochemical techniques, GC, and MS are the main techniques used to date to study these enzymes. Although these methods are well established, some measurement operations change the condition of the reaction system. Chemical indicators are also typically used for this purpose but may perturb the reaction system and cannot distinguish isotopes and nuclear spin isomers. I believe that the newly developed Raman method presented here is potentially useful and applicable in assaying various enzymatic reactions of gaseous substrates.

References

1. Lubitz W, Ogata H, Rüdiger O, Reijerse E (2014) Hydrogenases. *Chem. Rev.* 114:4081–4148.
2. Stephenson M, Stickland LH (1931) Hydrogenase: the reduction of sulphate to sulphide by molecular hydrogen. *Biochem. J.* 25:215.
3. Farkas A (1934) The decomposition of sodium formate by *Bacterium coli* in the presence of heavy water. *R. Soc.* 115:373–379.
4. Krasna AI, Rittenberg D (1954) The mechanism of action of the enzyme hydrogenase. *J. Am. Chem. Soc.* 76:3015–3020.
5. Tamiya N, Miller SL (1963) Kinetic studies on hydrogenase. *J. Biol. Chem.* 238:2194–2198.
6. Krasna AI (1979) Hydrogenase: properties and applications. *Enzyme Microb. Technol.* 1:165–172.
7. Vignais PM (2005) H/D exchange reactions and mechanistic aspects of the hydrogenases. *Coord. Chem. Rev.* 249:1677–1690.
8. Vogt S, Lyon EJ, Shima S, Thauer RK (2008) The exchange activities of [Fe] hydrogenase (iron-sulfur-cluster-free hydrogenase) from methanogenic archaea in comparison with the exchange activities of [FeFe] and [NiFe] hydrogenases. *J. Biol. Inorg. Chem.* 13:97–106.
9. Yagi T, Tsuda M, Inokuchi H (1973) Kinetic studies on hydrogenase: parahydrogen-orthohydrogen conversion and hydrogen-deuterium exchange reactions. *J. Biochem.* 73:1069–1081.
10. McTavish H, Sayavedra-Soto LA, Arp DJ (1996) Comparison of isotope exchange,

- H₂ evolution, and H₂ oxidation activities of *Azotobacter vinelandii* hydrogenase. *Biochim. Biophys. Acta (BBA)-Protein Struct. Mol. Enzymol.* 1294:183–190.
11. Arp DJ, Burris RH (1982) Isotope exchange and discrimination by the H₂-oxidizing hydrogenase from soybean root nodules. *Biochim. Biophys. Acta (BBA)-Protein Struct. Mol.* 700:7–15.
12. Fauque GD, Berlier YM, Czechowski MH, Dimon B, Lespinat PA, LeGall J (1987) A proton-deuterium exchange study of three types of *Desulfovibrio* hydrogenases. *J. Ind. Microbiol.* 2:15–23.
13. Leroux F, Dementin S, Burlat B, Cournac L, Volbeda A, Champ S, Martin L, Guigliarelli B, Bertrand P, Fontecilla-Camps J, et al. (2008) Experimental approaches to kinetics of gas diffusion in hydrogenase. *Proc. Natl. Acad. Sci.* 105:11188–11193.
14. Dementin S, Burlat B, De Lacey AL, Pardo A, Adryanczyk-Perrier G, Guigliarelli B, Fernandez VM, Rousset M (2004) A glutamate is the essential proton transfer gate during the catalytic cycle of the [NiFe] hydrogenase. *J. Biol. Chem.* 279:10508–10513.
15. Tai H, Xu L, Nishikawa K, Higuchi Y, Hirota S (2017) Equilibrium between inactive ready Ni-SI_r and active Ni-SI_a states of [NiFe] hydrogenase studied by utilizing Ni-SI_r-to-Ni-SI_a photoactivation. *Chem. Commun.* 53:10444–10447.
16. Ogata H, Nishikawa K, Lubitz W (2015) Hydrogens detected by subatomic resolution protein crystallography in a [NiFe] hydrogenase. *Nature* 520:571.
17. Yagi T, Ogo S, Higuchi Y (2014) Catalytic cycle of cytochrome-*c*₃ hydrogenase, a [NiFe]-enzyme, deduced from the structures of the enzyme and the enzyme mimic. *Int. J. Hydrogen Energy* 39:18543–18550.
18. Volbeda A, Charon M-H, Piras C, Hatchikian EC, Frey M, Fontecilla-Camps JC (1995) Crystal structure of the nickel-iron hydrogenase from *Desulfovibrio gigas*.

Nature 373:580.

19. Nicolet Y, Piras C, Legrand P, Hatchikian CE, Fontecilla-Camps JC (1999) *Desulfovibrio desulfuricans* iron hydrogenase: the structure shows unusual coordination to an active site Fe binuclear center. Structure 7:13–23.
20. Ogata H, Lubitz W, Higuchi Y (2009) [NiFe] hydrogenases: structural and spectroscopic studies of the reaction mechanism. Dalt. Trans.:7577–7587.
21. Yagi T, Higuchi Y (2013) Studies on hydrogenase. Proc. Japan Acad. Ser. B 89:16–33.
22. Shima S, Pilak O, Vogt S, Schick M, Stagni MS, Meyer-Klaucke W, Warkentin E, Thauer RK, Ermler U (2008) The crystal structure of [Fe]-hydrogenase reveals the geometry of the active site. Science 321:572–575.
23. Kalms J, Schmidt A, Frielingsdorf S, van der Linden P, von Stetten D, Lenz O, Carpentier P, Scheerer P (2016) Krypton derivatization of an O₂-tolerant membrane-bound [NiFe] hydrogenase reveals a hydrophobic tunnel network for gas transport. Angew. Chemie Int. Ed. 55:5586–5590.
24. Noor NDM, Matsuura H, Nishikawa K, Tai H, Hirota S, Kim J, Kang J, Tateno M, Yoon K-S, Ogo S, et al. (2018) Redox-dependent conformational changes of a proximal [4Fe-4S] cluster in Hyb-type [NiFe]-hydrogenase to protect the active site from O₂. Chem. Commun. 54:12385–12388.
25. Bertrand P, Dole F, Asso M, Guigliarelli B (2000) Is there a rate-limiting step in the catalytic cycle of [Ni-Fe] hydrogenases? J. Biol. Inorg. Chem. 5:682–691.
26. Hatchikian EC, Forget N, Fernandez VM, Williams R, Cammack R (1992) Further characterization of the [Fe]-hydrogenase from *Desulfovibrio desulfuricans* ATCC 7757. Eur. J. Biochem. 209:357–365.

27. Fontecilla-Camps JC, Amara P, Cavazza C, Nicolet Y, Volbeda A (2009) Structure-function relationships of anaerobic gas-processing metalloenzymes. *Nature* 460:814–822.
28. Montet Y, Amara P, Volbeda A, Vernede X, Hatchikian EC, Field MJ, Frey M, Fontecilla-Camps JC (1997) Gas access to the active site of Ni-Fe hydrogenases probed by X-ray crystallography and molecular dynamics. *Nat. Struct. Mol. Biol.* 4:523.
29. Abou Hamdan A, Dementin S, Liebgott PP, Gutierrez-Sanz O, Richaud P, De Lacey AL, Roussett M, Bertrand P, Cournac L, Léger C (2012) Understanding and tuning the catalytic bias of hydrogenase. *J. Am. Chem. Soc.* 134:8368–8371.
30. Evans RM, Brooke EJ, Wehlin SAM, Nomerotskaia E, Sargent F, Carr SB, Phillips SE V, Armstrong FA (2016) Mechanism of hydrogen activation by [NiFe] hydrogenases. *Nat. Chem. Biol.* 12:46.
31. Brickwedde FG, Scott RB, Taylor HS (1935) The difference in vapor pressures of *ortho* and *para* deuterium. *J. Chem. Phys.* 3:653–660.
32. Bonhoeffer KF, Harteck P (1929) Über Para-und Orthowasserstoff. *Z. Phys. Chem. B* 4:113–141.
33. Vignais PM, Henry M-F, Berlier Y, Lespinat PA (1982) Effect of pH on H-²H exchange, H₂ production and H₂ uptake, catalysed by the membrane-bound hydrogenase of *Paracoccus denitrificans*. *Biochim. Biophys. Acta (BBA)-Bioenergetics* 681:519–529.
34. Nishikawa K, Mochida S, Hiromoto T, Shibata N, Higuchi Y (2017) Ni-elimination from the active site of the standard [NiFe]-hydrogenase upon oxidation by O₂. *J. Inorg. Biochem.* 177:435–437.
35. Berlier Y, Lespinat PA, Dimon B (1990) A gas chromatographic-mass

- spectrometric technique for studying simultaneous hydrogen-deuteron exchange and para-ortho-hydrogen conversion in hydrogenases of *Desulfovibrio vulgaris* Hildenborough. *Anal. Biochem.* 188:427–431.
36. De Lacey AL, Santamaria E, Hatchikian EC, Fernandez VM (2000) Kinetic characterization of *Desulfovibrio gigas* hydrogenase upon selective chemical modification of amino acid groups as a tool for structure-function relationships. *Biochim. Biophys. Acta - Protein Struct. Mol. Enzymol.* 1481:371–380.
37. Cammack R, Fernandez VM, Hatchikian EC (1994) [5] Nickel-iron hydrogenase. *Methods Enzym.* 243:43–68.
38. Westley C, Fisk H, Xu Y, Hollywood KA, Carnell AJ, Micklefield J, Turner NJ, Goodacre R (2017) Real-time monitoring of enzyme-catalysed reactions using deep UV resonance Raman spectroscopy. :6983–6987.
39. Stoicheff BP (1957) High resolution Raman spectroscopy of gases: IX. spectra of H₂, HD, AND D₂. *Can. J. Phys.* 35:730–741.
40. Jouanneau Y, Kelley BC, Berlier Y, Lespinat PA, Vignais PM (1980) Continuous monitoring, by mass spectrometry, of H₂ production and recycling in *Rhodospseudomonas capsulata*. *J. Bacteriol.* 143:628–636.
41. Vignais PM, Cournac L, Hatchikian EC, Elsen S, Serebryakova L, Zorin N, Dimon B (2002) Continuous monitoring of the activation and activity of [NiFe] -hydrogenases by membrane-inlet mass spectrometry. *Int. J. Hydrogen Energy* 27:1441–1448.
42. Cournac L, Guedeney G, Peltier G, Vignais PM (2004) Sustained photoevolution of molecular hydrogen in a mutant of *Synechocystis* sp. strain PCC 6803 deficient in the type I NADPH-dehydrogenase complex. *J. Bacteriol.* 186:1737–1746.
43. Lubitz W, Tumas W (2007) Hydrogen: an overview. *Chem. Rev.* 107:3900–3903.

44. Kaur-Ghumaan S, Stein M (2014) [NiFe] hydrogenases: how close do structural and functional mimics approach the active site? *Dalt. Trans.* 43:9392–9405.
45. Ruff A, Szczesny J, Marković N, Conzuelo F, Zacarias S, Pereira IAC, Lubitz W, Schuhmann W (2018) A fully protected hydrogenase/polymer-based bioanode for high-performance hydrogen/glucose biofuel cells. *Nat. Commun.* 9:3675.
46. Schilter D, Camara JM, Huynh MT, Hammes-Schiffer S, Rauchfuss TB (2016) Hydrogenase Enzymes and Their Synthetic Models: The Role of Metal Hydrides. *Chem. Rev.* 116:8693–8749.
47. Yoshikawa S, Shimada A (2015) Reaction Mechanism of Cytochrome c Oxidase. *Chem. Rev.* 115:1936–1989.
48. Hoffman BM, Lukoyanov D, Yang Z-Y, Dean DR, Seefeldt LC (2014) Mechanism of Nitrogen Fixation by Nitrogenase: The Next Stage. *Chem. Rev.* 114:4041–4062.
49. Shiro Y (2012) Structure and function of bacterial nitric oxide reductases: nitric oxide reductase, anaerobic enzymes. *Biochim. Biophys. Acta (BBA)-Bioenergetics* 1817:1907–1913.
50. Tinberg CE, Lippard SJ (2011) Dioxygen Activation in Soluble Methane Monooxygenase. *Acc. Chem. Res.* 44:280–288.

Acknowledgement

I would like to express my sincere gratitude to Professor Yoshiki Higuchi of University of Hyogo (UH) for his helpful guidance, kind encouragements and fruitful discussions. My deep heartfelt appreciation goes to the late Professor Takashi Ogura of UH for his supports and inventive ideas for experimental design. I learned the philosophy on research from him. I am deeply grateful to Professor Tsunehiro Mizushima of UH, Professor Tohru Yoshihisa of UH, Professor Makoto Sakai of Okayama University of Science, Professor Syun-Ru Yeh of Albert Einstein College of Medicine, Professor Minoru Kubo of UH and Dr. Sachiko Yanagisawa of UH for their helpful discussions and encouragement. I am deeply grateful to Dr. Satoru Nakashima of Nara Institute of Science and Technology (NAIST) for his encouragement and guidance especially in the field of spectroscopy. Without his experience and deep knowledge, this research would not have proceeded. I am deeply grateful to Dr. Koji Nishikawa of UH for tons of insightful discussions, his continuous encouragement (by providing sweets, which make me gain weight) and his guidance for handling enzymes. Mr. Shota Inoue and Dr. Koji Nishikawa provide highly purified hydrogenase. I would like to thank Professor Takehiro Ohta of Sanyo-Onoda City University for insightful comments and warm encouragement. He kindly provides a spectrometer and a detector for my research. Professor Tatsuhiko Yagi of Shizuoka University gives me many insightful comments and suggestions. Discussions with Professors Yasuteru Shigeta of University of Tsukuba and Katsuyuki Fukutani of the University of Tokyo was fruitful for my research.

I owe my deepest gratitude to the students, graduates and stuffs belonging to both Higuchi's group and Kubo's group (formerly Ogura's), who give me supports and warm encouragement. Especially, I thank Dr. Naoki Shibata and Dr. Takeshi Hiromoto for helpful discussions, and Ms. Kiriko Hataguchi and Ms. Kayoko Matsumoto for bacterial cultures. Advice received from Professor Teizo Kitagawa of UH were very helpful for review my research. I thank the students and stuffs of picobiology course for their help. Especially, I thank students in the same year who encouraged each other by discussing research and private life issues.

I express my sincere gratitude to my parents, Takashi and Yoshiko Kawahara, and Shigemitsu and Akemi Nakagawa, for their understanding and hearty encouragements. Finally, I thank my husband, Takenari Nakagawa, who always cheered me and did almost all the housework while complaining.

Appendix I

Comparison of enzymatic activities of various hydrogenases

<i>species</i>	Type	H/D	exchange	H ₂ evolution	H ₂ uptake	additives	ref
		activity		$\mu\text{mol min}^{-1} \text{mg}^{-1}$	$\mu\text{mol min}^{-1} \text{mg}^{-1}$		
		$\mu\text{mol min}^{-1} \text{mg}^{-1}$					
<i>Thiocapsa roseopersicina</i>	[NiFe]	220		65	55	Methyl viologen	[1]
		(pH=5.5)		(pH=4.0)	(pH=9.5)		
<i>Azobacter vinelandii</i>	[NiFe]	34		32	-	dithionite	[1]
		(pH=5.0)		(pH=5.0)			
<i>Desulfovibrio fructosovorans</i>	[NiFe]	223		65 (pH=7.6)	330	no information	[1]
		(pH=5.5)			(pH=8.5)		
<i>Desulfovibrio vulgaris</i> Miyazaki F	[NiFe]	282		75600	50400	Cyt c ₃	[2]
		28		(pH=7)	(pH=7)		this method
<i>Desulfovibrio vulgaris</i> strain Hildenborough	[FeFe]	2700		4800	50000	no information	[3,4]
		(pH=5.0)		(pH=5.6-6.0)	(pH=8.4)		
<i>Desulfovibrio desulfuricans</i>	[FeFe]	3360				no information	[3,5]

[1]. Bertrand P, Dole F, Asso M, Guigliarelli B (2000) Is there a rate-limiting step in the catalytic cycle of [Ni-Fe] hydrogenases? J. Biol. Inorg. Chem. 5:682–691.

[2]. Yagi T, Tsuda M, Inokuchi H (1973) Kinetic studies on hydrogenase: parahydrogen-orthohydrogen conversion and hydrogen-deuterium exchange reactions. J. Biochem.

73:1069–1081.

[3]. Vogt S, Lyon EJ, Shima S, Thauer RK (2008) The exchange activities of [Fe] hydrogenase (iron-sulfur-cluster-free hydrogenase) from methanogenic archaea in comparison with the exchange activities of [FeFe] and [NiFe] hydrogenases. *J. Biol. Inorg. Chem.* 13:97–106.

[4]. Fauque GD, Berlier YM, Czechowski MH, Dimon B, Lespinat PA, LeGall J (1987) A proton-deuterium exchange study of three types of *Desulfovibrio* hydrogenases. *J. Ind. Microbiol.* 2:15–23.

[5]. Hatchikian EC, Forget N, Fernandez VM, Williams R, Cammack R (1992) Further characterization of the [Fe]-hydrogenase from *Desulfovibrio desulfuricans* ATCC 7757. *Eur. J. Biochem.* 209:357–365.

divided by 2 since HD should not split into D⁻ and H⁺, but should be divided into H⁻ and D⁺ to proceed from E(HD) to E(H₂). Assuming that the process towards either happens with the same probability, k is multiplied by 1/2 which is the probability of going in the direction of E(H₂) from E(HD).

Derivation of the rate equations

Using the reaction model depicted in Fig. 4–1, the analytical solution was derived as follows. The calculations have been already reported by Leroux *et al.* (ref 13 in main body) [D₂], [HD] and [H₂] are the concentration of dissolved gases. [D₂]₀ is the initial concentration of D₂. ([D₂]₀ = [D₂] + [HD] + [H₂]). [E], [E(D₂)], [E(HD)] and [E(H₂)] are the concentrations of enzymes that are corresponding to those defined above. The total concentration of enzyme is [E]₀ ([E]₀ = [E] + [E(D₂)] + [E(HD)] + [E(H₂)] since [E]₀ << [D₂]₀).

The differential equations are:

$$d[E]/dt = -k_{in} \times [E] \times ([D_2] + [HD] + [H_2]) + k_{out} ([E(D_2)] + [E(HD)] + [E(H_2)])$$

$$d[E(D_2)]/dt = k_{in} \times [E] \times [D_2] - (k + k_{out}) \times [E(D_2)]$$

$$d[E(HD)]/dt = k_{in} \times [E] \times [HD] + k \times [E(D_2)] - (k/2 + k_{out}) \times [E(HD)]$$

$$d[E(H_2)]/dt = k_{in} \times [E] \times [H_2] + k/2 \times [E(HD)] - k_{out} \times [E(H_2)]$$

$$d[D_2]/dt = -k_{in} \times [E] \times [D_2] + k_{out} \times [E(D_2)]$$

$$d[HD]/dt = -k_{in} \times [E] \times [HD] + k_{out} \times [E(HD)]$$

$$d[H_2]/dt = -k_{in} \times [E] \times [H_2] + k_{out} \times [E(H_2)]$$

The initial conditions were [D₂]₀ = 1, [HD]₀ = 0, [H₂]₀ = 0, [E] = [E]₀, [E(D₂)] = 0, [E(HD)] = 0 and [E(H₂)] = 0. The steady state values of [E], [E(D₂)], [E(HD)] and [E(H₂)]

are as follows:

$$[E] = [E]_0 / (1 + k'_{in} \times [D_2]_0)$$

$$[E(D_2)] = (k'_{in} \times [E]_0 \times [D_2]) / \{(1 + k'_{in} \times [D_2]_0) \times (1 + k')\}$$

$$[E(HD)] = \{k'_{in} \times [E]_0 \times 2 (k'[D_2] + (k' + 1)[HD])\} / \{(1 + k'_{in} \times [D_2]_0) \times (1 + k') \times (2 + k')\}$$

$$[E(H_2)] = \{k'_{in} \times [E]_0 \times (k'^2[D_2] + k'(k' + 1)[HD] + (1 + k')(2 + k')[H_2])\} / \{(1 + k'_{in} \times [D_2]_0) \times (1 + k') \times (2 + k')\}$$

$$k' = k/k_{out}$$

$$k'_{in} = k_{in}/k_{out}$$

From the differential equations and the solution above,

$$[D_2] = [D_2]_0 e^{-[k_a / (1+kb)] t}$$

$$[HD] = 2[D_2]_0 \{e^{-[k_a / (2+kb)] t} - e^{-[k_a / (1+kb)] t}\}$$

$$[H_2] = [D_2]_0 (1 - 2e^{-[k_a / (2+kb)] t} + e^{-[k_a / (1+kb)] t})$$

where $k_a = (k \times k_{in} \times [E]_0) / (k_{out} + k_{in} \times [D_2]_0)$, $k_b = k/k_{out}$, and $[E]_0$ is the enzyme concentration.

List of Figures and Tables

Figures

Chapter 1

Figure 1–1. Crystal structure of [NiFe] hydrogenase from *Desulfovibrio vulgaris* Miyazaki F. ...11

Figure 1–2. Proposed catalytic mechanism for the reversible oxidation of H₂ at the active site of [NiFe] hydrogenase. ...12

Figure 1–3. Comparison between conventional methods and Raman spectroscopy. ...17

Chapter 2

Figure 2–1. Plan view inside the spectrometer. ...23

Figure 2–2. Experimental setup. (A) Schematic illustration of the Raman spectroscopy-based assay system. (B) Schematic illustration of the water thermostatically controlled cuvette holder and the arrangement of the associated optical elements. (C) Custom-built reaction cuvette for anaerobic measurements of the reaction. The glass cuvette possesses four transparent surfaces for Raman measurements. ...26

Figure 2–3. Rotational–vibrational spectra of pure H₂ measured using the Raman system. ...29

Figure 2–4. Rotational–vibrational spectra of gaseous molecular hydrogen species (H₂, HD, and D₂) measured using the Raman spectroscopy-based assay system. ...32

Figure 2–5. Results of multipeak fitting for the rotational–vibrational spectra of normal D₂ and H₂. ...35

Chapter 3

Figure 3–1. Custom-built reaction cuvettes explained in Chapter 3. ...41

Chapter 4

Figure 4–1. Scheme of the H/D exchange reaction used for the kinetic analysis. ...56

Figure 4–2. H/D exchange reaction in the D₂/H₂O system catalyzed by [NiFe] hydrogenase from *Desulfovibrio vulgaris* Miyazaki F. (A) Waterfall plot of the Raman spectra during the H/D exchange reaction in the D₂/H₂O system. (B) Time course of the isotopic composition of molecular hydrogen. ...60

Figure 4–3. Kinetic analysis of the time course of the H/D exchange reaction catalyzed by [NiFe] hydrogenase. The time course of the reaction was measured at enzyme concentrations of 2, 5, 10, and 20 μM. ...61

Tables

Chapter 2

Table 2–I. Relationship between F-value and the Raman intensity, baseline, and signal-to-noise (S/N) ratio	...30
---	-------

Chapter 4

Table 4–I. H/D exchange activities for several enzyme concentrations	...62
---	-------

Table 4–II. τ_D for several volumes of reaction mixture at 10 μ M enzyme concentration	...62
--	-------

Table 4–III. τ_D , v_2/v_1 , k_a and k_b for several enzyme concentrations	...64
--	-------